THE EUROPEAN
PHYSICAL JOURNAL C

Regular Article - Theoretical Physics

$(g-2)_\mu$ and stau coannihilation: dark matter and collider analysis

Manimala Chakraborti[1,a] (ID)**, Sven Heinemeyer**[2,b]**, Ipsita Saha**[3,c]

[1] School of Physics and Astronomy, University of Southampton, Southampton SO17 1BJ, UK
[2] Instituto de Física Teórica (UAM/CSIC), Universidad Autónoma de Madrid, Cantoblanco, 28049 Madrid, Spain
[3] Department of Physics, Indian Institute of Technology Madras, Chennai 600036, India

Abstract Slepton coannihilation is one of the most promising scenarios that can bring the predicted Dark Matter (DM) abundance in the the Minimal Supersymmetric Standard Model (MSSM) into agreement with the experimental observation. In this scenario, the lightest supersymmetric particle (LSP), usually assumed to be the lightest neutralino, $\tilde{\chi}_1^0$ can serve as a Dark Matter (DM) candidate while the sleptons as the next-to-LSPs (NLSPs) lie close in mass. In our previous studies analyzing the electroweak sector of MSSM, a degeneracy between the three generations of sleptons was assumed for the sake of simplicity. In case of slepton coannihilation this directly links the smuons involved in the explanation for $(g-2)_\mu$ to the coannihilating NLSPs required to explain the DM content of the universe. On the other hand, in well-motivated top-down models such degeneracy do not hold, and often the lighter stau turns out to be the NLSP at the electroweak (EW) scale, with the smuons (and selectrons) somewhat heavier. In this paper we analyze such a scenario at the EW scale assuming non-universal slepton masses where the first two generations of sleptons are taken to be mass-degenerate and heavier than the staus, enforcing stau coannihilation. We analyze the parameter space of the electroweak MSSM in the light of a variety of experimental data namely, the DM relic density and direct detection limits, LHC data and especially, the discrepancy between the experimental result for the anomalous magnetic moment of the muon, $(g-2)_\mu$, and its Standard Model (SM) prediction. We find an upper limit on the lightest neutralino mass, the lighter stau mass and the mass of the tau sneutrino of about ~ 550 GeV. In contrast to the scenario with full degeneracy among the three families of sleptons, the upper limit on the light smuon/selectron mass moves up by ~ 200 GeV. We

analyze the DD prospects as well as the physics potential of the HL-LHC and a future high-energy e^+e^- collider to investigate this scenario further. We find that the combination DD experiments and e^+e^- collider searches with center of mass energies up to $\sqrt{s} \sim 1100$ GeV can fully cover this scenario.

1 Introduction

One of the main objectives in today's collider physics as well as "direct detection" (DD) searches is to understand the nature and origin of Dark Matter (DM). A leading candidate among the plethora of Beyond the Standard Model (BSM) theories that predict a viable DM particle is the Minimal Supersymmetric (SUSY) Standard Model (MSSM) [1–4] (see Ref. [5] for a recent review). MSSM extends the particle content of the Standard Model (SM) by predicting two scalar partners for all SM fermions as well as fermionic partners to all SM bosons. Furthermore, contrary to the SM case, the MSSM requires the presence of two Higgs doublets, resulting in five physical Higgs bosons instead of the single Higgs boson in the SM, namely the light and heavy $\mathcal{CP}$-even Higgs bosons, h and H, the $\mathcal{CP}$-odd Higgs boson, A, and a pair of charged Higgs bosons, $H^\pm$. The SUSY partners of the SM leptons and quarks are known as the scalar leptons and quarks (sleptons, squarks) respectively. The neutral SUSY partners of the neutral Higgses and electroweak (EW) gauge bosons give rise to the four neutralinos, $\tilde{\chi}_{1,2,3,4}^0$. The corresponding charged SUSY partners are the charginos, $\tilde{\chi}_{1,2}^\pm$. In an R-parity conserving scenario of MSSM the lightest neutralino can be the lightest SUSY particle (LSP), resulting in a good DM candidate. Depending on its nature, it can make up the full DM content of the universe [6,7], or only a fraction of it. In the latter case, an additional DM component is

ᵃ e-mail: M.Chakraborti@soton.ac.uk (corresponding author)

ᵇ e-mail: Sven.Heinemeyer@cern.ch

ᶜ e-mail: ipsita@iitm.ac.in

required, which could be, e.g., a SUSY axion [8], to saturate the experimentally measured relic density.

In Refs. [9–13] we performed a comprehensive analysis of the EW sector of the MSSM, taking into account all relevant theoretical and experimental constraints. The experimental results comprised in particular the deviation of the anomalous magnetic moment of the muon (either the previous result [9,10], or the new, stronger limits [11,12]),[1] the DM relic abundance [110] (either as an upper limit [10,12] or as a direct measurement [9,11,12]), the DM direct detection (DD) experiments [111–113] and the direct searches at the LHC [114,115]. In Refs. [9–12] we focused on the interplay of $(g-2)_\mu$, DM and future collider searches, while in Ref. [13] the MSSM prediction of the mass of the W boson [116–118] was analyzed.

Five different scenarios were analyzed in our previous works, classified by the mechanism that brings the LSP relic density into agreement with the measured values. The scenarios differ by the nature of the Next-to-LSP (NLSP), or equivalently by the hierarchies between the mass scales determining the neutralino, chargino and slepton masses. The relevant mass scales that determine such hierarchies are the gaugino soft SUSY-breaking parameters M_1 and M_2, the Higgs mixing parameter μ and the slepton soft SUSY-breaking parameters $m_{\tilde{l}_L}$ and $m_{\tilde{l}_R}$ (see Sect. 2 for a detailed description). The five scenarios can be summarized as follows [9–12]:

(i) bino/wino DM with $\tilde{\chi}_1^\pm$-coannihilation ($M_1 \lesssim M_2$): DM relic density can be fulfilled, $m_{\text{(N)LSP}} \lesssim 650\ (700)$ GeV;

(ii) bino DM with $\tilde{l}^\pm$-coannihilation case-L ($M_1 \lesssim m_{\tilde{l}_L}$): DM relic density can be fulfilled, $m_{\text{(N)LSP}} \lesssim 650\ (700)$ GeV;

(iii) bino DM with $\tilde{l}^\pm$-coannihilation case-R ($M_1 \lesssim m_{\tilde{l}_R}$): DM relic density can be fulfilled, $m_{\text{(N)LSP}} \lesssim 650\ (700)$ GeV.

(iv) higgsino DM ($\mu < M_1, M_2, m_{\tilde{l}_L}, m_{\tilde{l}_R}$): DM relic density is only an upper bound (the full relic density implies $m_{\tilde{\chi}_1^0} \sim 1$ TeV and $(g-2)_\mu$ cannot be fulfilled), $m_{\text{(N)LSP}} \lesssim 500$ GeV with $m_{\text{NLSP}} - m_{\text{LSP}} \sim 5$ GeV.

(v) wino DM ($M_2 < M_1, \mu, m_{\tilde{l}_L}, m_{\tilde{l}_R}$): DM relic density is only an upper bound, (the full relic density implies $m_{\tilde{\chi}_1^0} \sim 3$ TeV and $(g-2)_\mu$ cannot be fulfilled), $m_{\text{(N)LSP}} \lesssim 600$ GeV with $m_{\text{NLSP}} - m_{\text{LSP}} \sim 0.3$ GeV.[2]

In all the scenarios mentioned above, a degeneracy between the three generations of sleptons was assumed. Apart from the resulting simplicity of the analysis, such a degeneracy is also motivated by the solution to the SUSY flavour problem, which prefers the three generations of scalars to possess degenerate soft SUSY-breaking masses [121,122]. Within the scenarios (ii) and (iii) the assumed degeneracy directly links the smuons involved in the explanation for $(g-2)_\mu$ to the coannihilating NLSPs required to explain the DM content of the universe. On the other hand, in well-motivated top-down models with a specific high-scale SUSY-breaking mechanism (e.g. minimal supergravity (mSUGRA) [123]), there is no such degeneracy, and often the lighter stau becomes the NLSP at the EW scale with the smuons (and selectrons) somewhat heavier. This has been explored in the context of the Constrained MSSM (CMSSM) in, e.g., Refs. [124–127], and within the non-universal scalar mass models (NUHM) in, e.g., Ref. [128]. Consequently, a full mass degeneracy of the three slepton families should be regarded as an artificial constraint. Indeed, in Ref. [129] it was shown that leaving the third generation slepton masses independent of the first and second generations, as it had been done previously in Ref. [130], has a strong impact on the resulting phenomenology. Therefore, it is crucial to investigate this scenario in a general manner in the context of the EW MSSM in relation to updated collider, DM and $(g-2)_\mu$ constraints.

In this paper we analyze an MSSM scenario at the EW scale, assuming non-universality of the input slepton masses such that the smuons and selectrons remain mass-degenerate, whereas the staus turn out to be lighter. This makes the staus to be the NLSPs, enforcing stau coannihilation. As in the scenarios (ii) and (iii) we either require left- or the right-handed stau mass parameter to be close to M_1. For these two scenarios, corresponding more to a top-down model motivated mass hierarchy, we analyze the complementarity of DD experiments and future collider experiments, concretely the HL-LHC and a possible future linear e^+e^- collider, the International Linear Collider (ILC) operated at a center-of-mass energy of up to $\sqrt{s} \lesssim 1$ TeV, the ILC1000. In the first step we analyze the predictions for the DM relic density as a function of the (N)LSP masses. We show the results both for DM fulfilling the relic density as well as taking the DM density only as an upper bound. In the second step we evaluate the prospects for future DD experiments in these two scenarios. We show that both scenarios can result in DD cross sections below the neutrino floor for a significant amount of model parameter space with the DM relic density remaining substantially below the Planck measurement. In this case direct searches at the HL-LHC and particularly at the ILC1000 will be necessary to fully probe these scenarios.

---

[1] Other evaluations of $(g-2)_\mu$ within the framework of SUSY using the new combined deviation Δa_μ (see Sect. 3) can be found in Refs. [14–109].

[2] It should be noted that this scenario requires special care concerning the correct choice of the chargino/neutralino renormalization scheme, see Refs. [119,120] and the corresponding discussion in Ref. [10].

The plan of the paper is as follows. In Sect. 2 we briefly review the parameters of the EW sector of MSSM. The relevant constraints for this analysis are outlined in Sect. 3. Section 4 contains the details of our parameter scan strategy and analysis flow. Our results are described in Sect. 5. Finally, we summarize in Sect. 6.

2 The electroweak sector of the MSSM

In our MSSM notation we follow exactly Ref. [9], with the exception of the degeneracy of the slepton mass parameters. We restrict ourselves here to a very short introduction of the relevant symbols and parameters, concentrating on the EW sector of the MSSM. This sector consists of charginos, neutralinos and scalar leptons. Concerning the scalar quark sector, we simply assume it to be heavy such that it does not play a relevant role in our analysis. Furthermore, throughout this paper we also assume the absence of $\mathcal{CP}$-violation, i.e. that all parameters are real.

The masses and mixings of the four neutralinos are given (on top of SM parameters) by the $SU(2)_L$ and $U(1)_Y$ gaugino masses, M_2 and M_1, the Higgs mixing parameter μ, as well as $\tan\beta := v_2/v_1$: the ratio of the two vacuum expectation values (vevs) of the two Higgs doublets. After diagonalizing the mass matrix the four eigenvalues yield the four neutralino masses $m_{\tilde{\chi}_1^0} < m_{\tilde{\chi}_2^0} < m_{\tilde{\chi}_3^0} < m_{\tilde{\chi}_4^0}$. Similarly, the masses and mixings of the charginos are given (on top of SM parameters) by M_2, μ and $\tan\beta$. Diagonalizing the mass matrix yields the two chargino-mass eigenvalues $m_{\tilde{\chi}_1^\pm} < m_{\tilde{\chi}_2^\pm}$.

For the sleptons, contrary to Refs. [9–12], we have chosen common soft SUSY-breaking parameters for the first two generations, but different for the third generation. The charged selectron and smuon mass matrices are given (on top of SM parameters) by the diagonal soft SUSY-breaking parameters $m_{\tilde{l}_L}^2$ and $m_{\tilde{l}_R}^2$ and the trilinear Higgs-slepton coupling A_l ($l = e, \mu$), where the latter are set to zero. Correspondingly, the stau mass matrix is given in terms of $m_{\tilde{\tau}_L}$, $m_{\tilde{\tau}_R}$ and A_τ. The latter is scanned over a range of values determined by the vacuum stability constraints, $A_\tau^2 + 3\mu^2 < 7.5(m_{\tilde{\tau}_L}^2 + m_{\tilde{\tau}_R}^2)$, allowing for the possibility of a metastable universe [131–134].

The mixing between the "left-handed" and "right-handed" sleptons is only relevant for staus, where the off-diagonal entry in the mass matrix is given by $-m_\tau \mu \tan\beta$. Consequently, for the first two generations, the mass eigenvalues can be approximated as $m_{\tilde{l}_1} \simeq m_{\tilde{l}_L}, m_{\tilde{l}_2} \simeq m_{\tilde{l}_R}$ (assuming small D-terms). We do not mass order the sleptons, i.e. we follow the convention that $\tilde{l}_1$ ($\tilde{l}_2$) has the large "left-handed" ("right-handed") component. As symbols for the first and second generation masses we use $m_{\tilde{l}_1}$ and $m_{\tilde{l}_2}$. We also use symbols for the scalar electron, muon and tau masses indi-

vidually, $m_{\tilde{e}_{1,2}}$, $m_{\tilde{\mu}_{1,2}}$ and $m_{\tilde{\tau}_{1,2}}$. The sneutrino and slepton masses are connected by the usual SU(2) relation.

Overall, the EW sector at the tree level can be described with the help of nine parameters: M_2, M_1, μ, $\tan\beta$, $m_{\tilde{l}_L}$, $m_{\tilde{l}_R}$, $m_{\tilde{\tau}_L}$, $m_{\tilde{\tau}_R}$ and A_τ. We assume μ, M_1, $M_2 > 0$ throughout our analysis. In Ref. [9] it was shown that this covers the relevant parameter space once the $(g-2)_\mu$ results are taken into account (see, however, the discussion in Ref. [26]).

Following the experimental limits for strongly interacting particles from the LHC [114,115], we assume that the colored sector of the MSSM is substantially heavier than the EW sector, and therefore does not play a role in our analysis. For the Higgs-boson sector we assume that the radiative corrections to the light $\mathcal{CP}$-even Higgs boson, originating largely from the top/stop sector, yield a value in agreement with the experimental data, $M_h \sim 125$ GeV. This naturally yields stop masses in the TeV range [129,135], in agreement with the LHC bounds. Concerning the heavy Higgs-boson mass scale, M_A (the $\mathcal{CP}$-odd Higgs-boson mass), we have shown in Refs. [9–12] that A-pole annihilation is largely excluded. Consequently, we also here assume M_A to be sufficiently large to not play a role in our analysis.

3 Relevant constraints

The SM prediction of a_μ is given by [136] (based on Refs. [137–156]),

$$a_\mu^{\text{SM}} = (11659181.0 \pm 4.3) \times 10^{-10} . \tag{1}$$

After the publication of the last results from the Muon g-2 Theory Initiative [136], a lattice calculation [157] for the leading order hadronic vacuum polarization (LO HVP) contribution has appeared yielding a somewhat higher value for the a_μ^{SM}. While this result is partially supported by some other lattice calculations [158,159], a consensus among the various lattice groups is yet to be established. On the other hand, no new SM theory prediction has been published so far. In this analysis, we do not take the lattice result into account, and use Eq. (1) for the theoretical SM prediction of a_μ (see also the discussions in Refs. [9,157,160–163]).[3]

The combined experimental world average, based on Refs. [164,165], is given by

$$a_\mu^{\text{exp}} = (11659206.1 \pm 4.1) \times 10^{-10} . \tag{2}$$

---

[3] On the other hand, it is obvious that our conclusions would change substantially if the result presented in [157] turned out to be correct.

Compared with the SM prediction in Eq. (1), one finds a deviation of

$$\Delta a_\mu = (25.1 \pm 5.9) \times 10^{-10} , \tag{3}$$

corresponding to a $4.2\,\sigma$ discrepancy. We use this limit as a cut at the $\pm 2\,\sigma$ level.

In the MSSM the main contribution to $(g-2)_\mu$ originates from one-loop diagrams involving $\tilde{\chi}_1^0 - \tilde{\mu}$ and $\tilde{\chi}_1^\pm - \tilde{\nu}$ loops [166–169]. In our analysis the MSSM contribution to $(g-2)_\mu$ is based on a full one-loop plus partial two-loop calculation [170–172] (see also [173,174]), as implemented into the code GM2Calc [175].

All other constraints are taken into account exactly as in Ref. [9–12]. These are:

- Vacuum stability constraints:
  Our parameter scan ranges (see Eqs. (6) and (7)) are determined keeping the vacuum stability constraint in mind. On top of that, all points are checked to possess a correct and stable EW vacuum, e.g. avoiding charge and color breaking minima, employing the public code Evade [134,176].
- Constraints from the LHC: All relevant SUSY searches for EW particles are taken into account, mostly via CheckMATE[177–179] (see Ref. [9] for details on many analyses newly implemented by our group). In the following we briefly review the relevance of various LHC searches for the present analysis.

  - The production of $\tilde{\chi}_1^\pm - \tilde{\chi}_2^0$ pairs leading to three leptons and $\not{E}_T$ in the final state [180,181]. We have implemented in CheckMATE the chargino-neutralino pair production searches in final states with three leptons and missing transverse momentum from Ref. [181]. We have included only the on-shell WZ selection which is the most important mode for our analysis.
  - Slepton-pair production leading to two same flavour opposite sign leptons and $\not{E}_T$ in the final state [182].
  - The ATLAS and CMS searches for direct stau pair production target the mass gap region $m_{\tilde{\tau}_{L,R}} - m_{\tilde{\chi}_1^0} \gtrsim$ 100 GeV [183–185]. This bound may, in principle, be relevant for the pair production of the heavier staus i.e. $\tilde{\tau}_R$ ($\tilde{\tau}_L$) for stau-L (stau-R) case (see Sect. 5). However, we have explicitly checked that after the application of $(g-2)_\mu$, DM and LHC constraints mentioned above, the surviving parameter points in our scans stay beyond the sensitivity reach of the stau pair production seraches.
  The pair production of $\tilde{\chi}_1^\pm - \tilde{\chi}_2^0$ pairs decaying via staus [185] may be effective in constraining our

parameter space. However, the decay products from the lighter stau, the coannihilation partner of the $\tilde{\chi}_1^0$, will be too soft to be detected by these searches. Thus, only the heavier one of the two staus may contribute to the signal cross section, provided the decay of $\tilde{\chi}_1^\pm - \tilde{\chi}_2^0$ via stau is kinematically allowed. Filtering out the parameter points for which the heavier stau is lighter than $\tilde{\chi}_1^\pm$ and $\tilde{\chi}_2^0$, we observed that only a handful points in the low $\tilde{\chi}_1^\pm / \tilde{\chi}_2^0$ mass region may potentially be affected by this constraint. A detailed account of the impact of the stau searches [185] on our parameter space is reserved for a future analysis. The latest bounds from the compressed stau searches are far too weak at present to be of relevance for our analysis [186].

  - The low mass gap between the third generation sleptons and the lightest neutralino in our analysis may give rise to long lived staus which are subject to bounds from dedicated long-lived particle (LLP) searches at the LHC. The ATLAS collaboration has looked for a heavy stable charged particle (HSCP) through specific ionisation energy loss in the detector [187,188]. The results have been interpreted for the pair production of staus in a gauge mediated SUSY-breaking scenario (GMSB) assuming stable staus (see Sect. 5.3 for detail). Since the search strategy is largely independent of the undelying model assumption, this limit can be applied to constrain the long lived staus in our model. The disappearing track searches [189,190] are targeted towards long-lived winos or higgsinos with production cross-section much larger compared to the staus. Thus, this search is ineffective in constraining our model parameter space. Our scenario remains equally unaffected by the displaced lepton searches [184,191] which requires a high-p_T displaced lepton in the signal events, following the theoretical framework of GMSB scenarios.

- Dark matter relic density constraints:
  the latest result from Planck [110] provides the experimental data. The relic density is given as

$$\Omega_{\text{CDM}} h^2 = 0.120 \pm 0.001 , \tag{4}$$

which we use as a measurement of the full MSSM density, or as an upper bound (evaluated with the central value plus 2σ),

$$\Omega_{\text{CDM}} h^2 \leq 0.122 . \tag{5}$$

The evaluation of the relic density in the MSSM is performed with MicrOMEGAs[192–195].

- Direct detection constraints of Dark matter:
  In comparison to previous analyses we use an updated limit on the spin-independent (SI) DM scattering cross-section σ_p^{SI} from the LZ [196] experiment (which are always substantially more relevant than the spin-dependent limits). The theoretical predictions are evaluated using the public code MicrOMEGAs[192–195]. Apart from this limit we will discuss the impact of possible future limits and the neutrino floor below.
  For parameter points with $\Omega_{\tilde{\chi}} h^2 \leq 0.118$ (i.e. lower than the 2σ lower limit from Planck [110], see Eq. (5)) the DM scattering cross-section is rescaled with a factor of $(\Omega_{\tilde{\chi}} h^2/0.118)$. This takes into account the fact that $\tilde{\chi}_1^0$ provides only a fraction of the total DM relic density of the universe.

Another potential set of constraints is given by the indirect detection of DM. However, we do not impose these constraints on our parameter space because of the well-known large uncertainties associated with astrophysical factors like DM density profile as well as theoretical corrections, see Refs. [197–200]. The most precise indirect detection limits come from DM-rich dwarf spheroidal galaxies, where the uncertainties on the cross section limits are found in the range of $\sim 2-3$ (from the lowest to the highest cross section limit) [201,202]. The most recent analysis [201], assuming the annihilation goes into one single mode (which is too "optimistic" for our scenarios), sets limits of $m_{\tilde{\chi}_1^0} \gtrsim 100$ GeV for the generic thermal relic saturating Eq. (4). However, this is well below our preferred parameter space (see next sections below). Additionally, it has been noted previously [203,204] that the indirect detection cross section of the DM for the stau coannihilation scenario lies almost two orders of magnitude below the current limits from Fermi-LAT [201]. Consequently, we do not further consider the indirect detection constraints in our analysis.

4 Parameter scan and analysis flow

4.1 Parameter scan

We scan the EW MSSM parameter space, fully covering the allowed regions of the relevant neutralino, chargino, stau and first/second generation slepton masses. We follow the approach taken in Refs. [9–12] and investigate the two scenarios of stau coannihilation discussed in Sect. 1. They are given by the possible mass orderings of $M_1 < M_2, \mu$, and $m_{\tilde{\tau}_L}, m_{\tilde{\tau}_R}$. These masses yield a bino-like LSP and fix the NLSP, thus ensuring stau coannihilation as the mechanism that reduces the relic DM density in the early universe to or below the current value (see Eqs. (4), (5)). We do not consider the possibility of pole annihilation, e.g. with the h, the

A or the Z boson. As argued in Refs. [9–12] these are rather remote possibilities in our set-up.[4]

As indicated above, we choose M_1 to be the smallest mass parameter and require that a scalar tau is close in mass. In this scenario "accidentally" the wino or higgsino component of the $\tilde{\chi}_1^0$ can be non-negligible in some parts of the parameter space. However, this is not a distinctive feature of this scenario. We distinguish two cases: either the SU(2) doublet staus, or the singlet staus are close in mass to the LSP.

stau-L: bino DM with $\tilde{\tau}_1$-coannihilation (SU(2) doublet)

$$100 \text{ GeV} \leq M_1 \leq 1000 \text{ GeV} , \ 1.2\,M_1 \leq M_2 \leq 10\,M_1 ,$$
$$1.2\,M_1 \leq \mu \leq 10\,M_1, \ 5 \leq \tan\beta \leq 60 ,$$
$$M_1 \leq m_{\tilde{\tau}_L} \leq 1.2\,M_1, m_{\tilde{\tau}_L} \leq m_{\tilde{\tau}_R} \leq 10\,m_{\tilde{\tau}_L} ,$$
$$1.2\,M_1 \leq m_{\tilde{l}_L}, m_{\tilde{l}_R} \leq 2 \text{ TeV} ,$$
$$A_\tau^2 \leq 7.5(m_{\tilde{\tau}_L}^2 + m_{\tilde{\tau}_R}^2) - 3\mu^2 . \tag{6}$$

stau-R: bino DM with $\tilde{\tau}_2$-coannihilation (SU(2) singlet)

$$100 \text{ GeV} \leq M_1 \leq 1000 \text{ GeV} , \ 1.2M_1 \leq M_2 \leq 10M_1 ,$$
$$1.2M_1 \leq \mu \leq 10M_1, \ 5 \leq \tan\beta \leq 60 ,$$
$$m_{\tilde{\tau}_R} \leq m_{\tilde{\tau}_L} \leq 10m_{\tilde{\tau}_R}, \ M_1 \leq m_{\tilde{\tau}_R} \leq 1.2M_1 ,$$
$$1.2M_1 \leq m_{\tilde{l}_L}, m_{\tilde{l}_R} \leq 2 \text{ TeV} ,$$
$$A_\tau^2 \leq 7.5(m_{\tilde{\tau}_L}^2 + m_{\tilde{\tau}_R}^2) - 3\mu^2 . \tag{7}$$

In both scans we choose flat priors of the parameter space and generate $\mathcal{O}(10^7)$ points. In order to obtain reliable *upper* limits on the (N)LSP masses, we performed dedicated scans in the respective parameter regions. These appear as more densely populated regions in the plots below.

As discussed above, the mass parameters of the colored sector have been set to high values, moving these particles outside the reach of the LHC. The mass of the lightest $\mathcal{CP}$-even Higgs-boson is in agreement with the LHC measurements of the ~ 125 GeV (concrete values are not relevant for our analysis). Similarly, M_A has been set to be above the TeV scale (see above).

4.2 Analysis flow

The two data samples were generated by scanning randomly over the input parameter ranges given above, assuming a flat prior for all parameters. We use the code SuSpect-v2.43 [205,206] as spectrum and SLHA file generator. In this step we ensure that all points satisfy the $\tilde{\chi}_1^\pm$ and slepton mass limits from LEP [207]. The SLHA output files as generated by SuSpect are then passed as input files to MicrOMEGAs-v5.2.13 and GM2Calc-v2.1.0 for the calculation of

---

[4] Concretely, we have set $M_A = 1.5$ TeV, ensuring that the heavy Higgs-boson sector does not play a role in our analysis.

the DM observables and $(g-2)_\mu$ respectively. The parameter points that satisfy the $(g-2)_\mu$ constraint of Eq. (3), the DM relic density constraint of Eqs. (4) or (5), the DD constraints (possibly with a rescaled cross section) and the vacuum stability constraints, tested with Evade, are then passed to the final check against the LHC constraints as implemented in CheckMATE. The relevant branching ratios of the SUSY particles (required by CheckMATE) are calculated using SDECAY-v1.5a [208].

5 Results

We follow the analysis flow as described above and denote the points surviving certain constraints with different colors:

- grey (round): all scan points.
- green (round): all points that are in agreement with $(g-2)_\mu$, taking into account the limit as given in Eq. (3), but are excluded by the DM relic density.
- blue (triangle): points that additionally give the correct relic density, see Sect. 3, but are excluded by the DD constraints.
- cyan (diamond): points that additionally pass the DD constraints, see Sect. 3, but are excluded by the LHC constraints.
- red (star): points that additionally pass the LHC constraints, see Sect. 3.

5.1 Upper limits and preferred parameter ranges: Stau-L case

We start our phenomenological analysis with the case of bino DM with $\tilde{\tau}_1$-coannihilation. In this scenario the $m_{\tilde{\tau}_L}$ parameter is close to M_1, defining the NLSP and the coannihilation mechanism. We refer to this scenario as the stau-L case.

In Fig. 1 we show the result of our parameter scan in the $m_{\tilde{\chi}_1^0}$–$m_{\tilde{\tau}_1}$ plane (left) and the $m_{\tilde{\chi}_1^0}$–$\Delta m_{\tilde{\tau}_1}$ plane ($\Delta m_{\tilde{\tau}_1} := m_{\tilde{\tau}_1} - m_{\tilde{\chi}_1^0}$, right plot). In the left plot the points are found by definition close to the diagonal. The extra scan region is clearly visible around $m_{\tilde{\chi}_1^0} \sim 600$ GeV in green, i.e. in agreement with $(g-2)_\mu$. The fact that our scan is effectively exhaustive w.r.t. $(g-2)_\mu$ can be understood simply by looking at the lower plot of Fig. 3 (see below), where we depict our scanned points in $m_{\tilde{\chi}_1^0} - \tan\beta$ plane. The upper limit on $m_{\tilde{\chi}_1^0}$ from $(g-2)_\mu$ is expected to be reached for the largest value of $\tan\beta$ in our scans i.e. $\tan\beta \approx 60$. By looking at the general behaviour of the points it can be inferred that the points can go at the most up to $m_{\tilde{\chi}_1^0} \approx 660$ GeV, saturating $\tan\beta \approx 60$. Thus, the $m_{\tilde{\chi}_1^0}$ range not covered in the scans amounts to ~ 20 GeV. Furthermore, since the final surviving points (red) indicate a clear upper limit, we refrained from

scanning for even higher $m_{\tilde{\chi}_1^0}$ values. The most restrictive constraint after the application of $(g-2)_\mu$ comes in the next step, i.e. with the requirement of correct relic density (dark blue+cyan+red points). This sets an upper limit on $m_{\tilde{\chi}_1^0}$ and $m_{\tilde{\tau}_1}$ of ~ 550 GeV. As can be seen in the right plot, the relic density constraint also requires a small mass splitting, which is decreasing with increasing $m_{\tilde{\chi}_1^0}$. This is similar to the "stau coannihilation strip" discussed in Ref. [209]. The only exception are a few points for $m_{\tilde{\chi}_1^0} \lesssim 300$ GeV where the mass difference can be relatively larger. These points correspond to a substantial bino-higgsino and/or bino-wino mixing, making stau coannihilation only a subdominant component of the total annihilation cross-section. As we go towards higher $m_{\tilde{\chi}_1^0}$, $\tan\beta$ becomes restricted to larger values, determining the mass difference between $\tilde{\chi}_1^0$ the $\tilde{\tau}_1$. The application of DD constraints (cyan+red points), does not have an impact on the allowed parameter space in the $m_{\tilde{\chi}_1^0}$-$m_{\tilde{\tau}_1}$ plane, except for cutting away the points $m_{\tilde{\chi}_1^0} \lesssim 300$ GeV with larger mass differences. For these points, the proximity of M_1, μ and/or M_2 makes the σ_p^{SI} sufficiently large [210] so that they are excluded by the LZ [196] bounds. Finally, the LHC constraints cut away mainly points with low $m_{\tilde{\chi}_1^0}$, resulting in the red points which are in agreement with all available constraints. Overall, we find $m_{(N)LSP} \lesssim 550$ GeV and $\Delta m_{\tilde{\tau}_1} \lesssim 30$ GeV.

The results look very similar in the $m_{\tilde{\chi}_1^0}$-$m_{\tilde{\nu}_\tau}$ plane and $m_{\tilde{\chi}_1^0}$-$\Delta m_{\tilde{\nu}_\tau}$ plane ($\Delta m_{\tilde{\nu}_\tau} := m_{\tilde{\nu}_\tau} - m_{\tilde{\chi}_1^0}$), as show in the left and right plots of Fig. 2 respectively. Compared to Fig. 1, here somewhat larger mass differences are found for the smaller $m_{\tilde{\chi}_1^0}$ values. However, the upper bound found is similar as in Fig. 1, $m_{\tilde{\nu}_\tau} \lesssim 550$ GeV.

Next, in Fig. 3 we show the results of our parameter scan in the $m_{\tilde{\chi}_1^0}$–$m_{\tilde{\mu}_1}$ plane (top left), the $m_{\tilde{\chi}_1^0}$–$m_{\tilde{\chi}_1^\pm}$ plane (top right) and the $m_{\tilde{\chi}_1^0}$–$\tan\beta$ plane (bottom). Since we enforce $\tilde{\tau}_1$-coannihilation, the other masses are effectively free. However, the combination of $(g-2)_\mu$ and LHC constraints still yield an upper limit on the lighter smuon mass of $m_{\tilde{\mu}_1} \lesssim 800$ GeV, i.e. only about ~ 100 GeV higher than in the case of $\tilde{\mu}_1$-coannihilation [11]. On the other hand, the lighter chargino mass driven by M_2 and μ, corresponds to hardly any upper limit and values exceeding ~ 3 TeV are found.

We finish our analysis of the $\tilde{\tau}_1$-coannihilation case with the $m_{\tilde{\chi}_1^0}$-$\tan\beta$ plane presented in the lower plot of Fig. 3. The $(g-2)_\mu$ constraint is fulfilled in a triangular region with largest neutralino masses allowed for the largest $\tan\beta$ values (where we stopped our scan at $\tan\beta = 60$). In agreement with the previous plots, the largest values for the lightest neutralino masses allowed by all the constraints are ~ 550 GeV. The LHC constraints cut out points at low $m_{\tilde{\chi}_1^0}$, nearly independent of $\tan\beta$, but disallowing all points
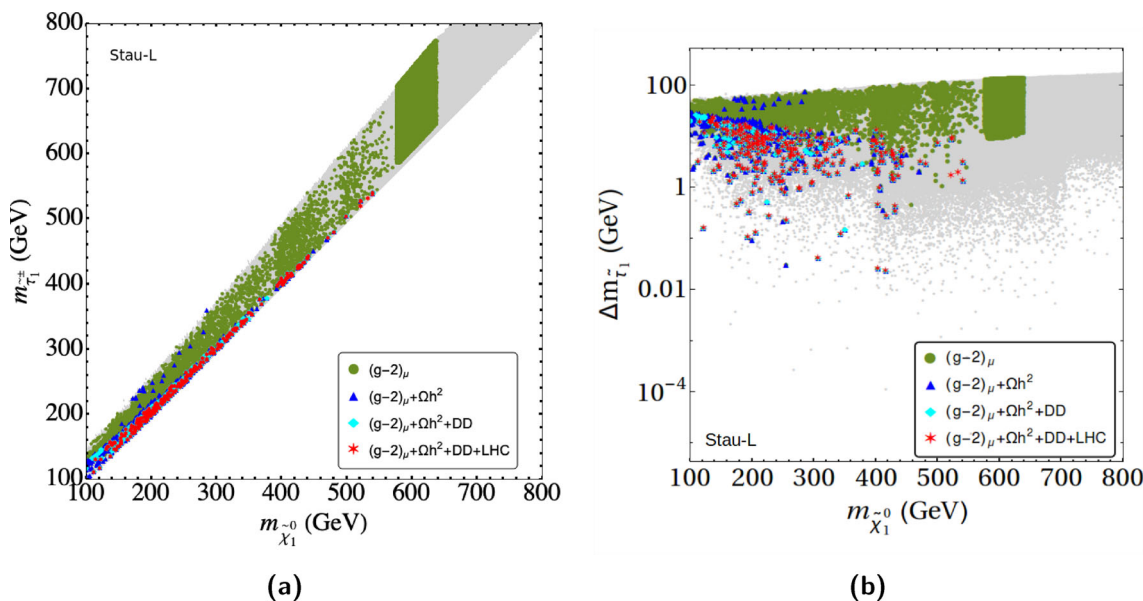
Fig. 1 The results of our parameter scan in the $\tilde{\tau}_1$ coannihilation case in the $m_{\tilde{\chi}_1^0}$–$m_{\tilde{\tau}_1}$ plane (left) and the $m_{\tilde{\chi}_1^0}$–$\Delta m_{\tilde{\tau}_1}$ plane ($\Delta m_{\tilde{\tau}_1} = m_{\tilde{\tau}_1} - m_{\tilde{\chi}_1^0}$, right plot). For the color coding: see text
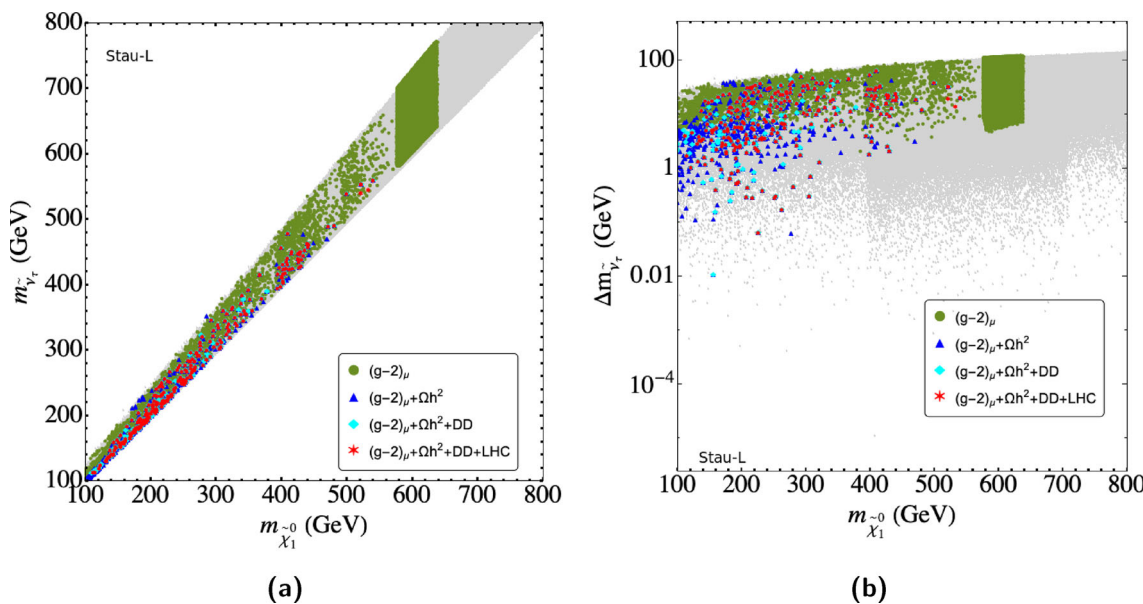

Fig. 2 The results of our parameter scan in the $\tilde{\tau}_1$-coannihilation case in the $m_{\tilde{\chi}_1^0}$–$m_{\tilde{\nu}_\tau}$ plane (left) and the $m_{\tilde{\chi}_1^0}$–$\Delta m_{\tilde{\nu}_\tau}$ plane ($\Delta m_{\tilde{\nu}_\tau} = m_{\tilde{\nu}_\tau} - m_{\tilde{\chi}_1^0}$)

with $\tan \beta \lesssim 15$. One can observe that points with masses of $m_{\tilde{\chi}_1^0} \sim m_{\tilde{\tau}_2} \sim 120$ GeV are still allowed by the LHC searches. As mentioned in Sect. 3, the current sensitivity of the compressed stau searches [186] are not sufficiently high to provide any constraint on our parameter space. Although slepton pair production searches [182] are able to provide some constraints, the limits from the $\tilde{\chi}_1^\pm - \tilde{\chi}_2^0$ pair production searches [180,181] gets relaxed because of the substantially large branching fraction of the $\tilde{\chi}_1^\pm$ and $\tilde{\chi}_2^0$ via the staus. In this plot we also show as a black line the bound from the

latest ATLAS search for heavy neutral Higgs bosons [211] in the channel $pp \to H/A \to \tau\tau$ in the $M_h^{125}(\tilde{\chi})$ benchmark scenario [212].[5] The black line in the plane has been obtained setting $m_{\tilde{\chi}_1^0} = M_A/2$, i.e. roughly to the requirement for A-pole annihilation, where points above the black lines are experimentally excluded. There are no points pass-

---

[5] This bound is based on the full Run 2 data from ATLAS, using the version 5 of `HiggsBounds` [213–218]. Subsequently, a corresponding limit from CMS was published [219], which is somewhat stronger in particular for lower Higgs mass values, strengthening our argument.

ing the current $(g-2)_\mu$ constraint below the black A-pole line. Consequently, A-pole annihilation can be considered as excluded in this scenario.

5.2 Upper limits and preferred parameter ranges: Stau-R case

The second part of our phenomenological analysis is the case of bino DM with $\tilde{\tau}_2$-coannihilation. In this scenario, referred to as the stau-R case, the $m_{\tilde{\tau}_R}$ parameter is close to M_1, defining the NLSP and the coannihilation mechanism.

In Fig. 4 we show the result of our parameter scan in the $m_{\tilde{\chi}_1^0}$–$m_{\tilde{\tau}_2}$ plane (left) and the $m_{\tilde{\chi}_1^0}$–$\Delta m_{\tilde{\tau}_2}$ plane ($\Delta m_{\tilde{\tau}_2} := m_{\tilde{\tau}_2} - m_{\tilde{\chi}_1^0}$, right plot). In the left plot, as in the stau-L case, the points are found by definition close to the diagonal. Once again, one can clearly see the densely scanned region around $m_{\tilde{\chi}_1^0} \sim 600$ GeV in green, i.e. in agreement with $(g-2)_\mu$. The same conclusions as for the stau-L case holds also in this case. The requirement of correct relic density sets an upper limit on $m_{\tilde{\chi}_1^0}$ and $m_{\tilde{\tau}_2}$ of ~ 550 GeV. As can be seen in the right plot, the relic density constraint requires a small mass splitting, $\Delta m_{\tilde{\tau}_2} \lesssim 10$ GeV. As in the stau-L case, a few atypical points with larger mass differences are found for $m_{\tilde{\chi}_1^0} \lesssim 300$ GeV, where the mixing among bino, wino and higgsino can be relatively large. This results in their exclusion by the DD constraints (cyan+red). Finally, the LHC constraints have hardly any impact on the allowed parameter space. Even points with masses of $m_{\tilde{\chi}_1^0} \sim m_{\tilde{\tau}_2} \sim 120$ GeV are permitted by the latest LHC constraints for reasons similar to those described in the ontext of the stau-L scenario. Overall, we find $m_{(\mathrm{N})\mathrm{LSP}} \lesssim 550$ GeV and $\Delta m_{\tilde{\tau}_2} \lesssim 10$ GeV.

Next, in Fig. 5 we show the results our parameter scan in the $m_{\tilde{\chi}_1^0}$–$m_{\tilde{\mu}_1}$ plane (top left), the $m_{\tilde{\chi}_1^0}$–$m_{\tilde{\chi}_1^\pm}$ plane (top right) and the $m_{\tilde{\chi}_1^0}$–$\tan\beta$ plane (bottom). The results are very similar to the stau-L case, and we refrain here from detailing them. Overall, we find $m_{\tilde{\mu}_1} \lesssim 800$ GeV, about about ~ 100 GeV higher than in the case of $\tilde{\mu}_2$-coannihilation [11]. For the chargino mass we find $m_{\tilde{\chi}_1^\pm} \lesssim 3$ TeV. Also the results in the $m_{\tilde{\chi}_1^0}$–$\tan\beta$ plane are very similar, but now we find $\tan\beta \gtrsim 25$. In this case also the A-pole annihilation can be considered as excluded in this scenario.

5.3 Stau finite life time

In this section we discuss the impact of the small mass difference between the $\tilde{\chi}_1^0$ LSP and the $\tilde{\tau}$ NLSP, which can lead to a "finite stau life time". To show the impact of the LLP and stable particle[6] searches at the LHC on our parameter space, we calculate the lifetime of the staus following

Ref. [220].[7] The results are shown in Fig. 6, in lifetime vs. $\Delta m = m_{\tilde{\tau}_{1,2}} - m_{\tilde{\chi}_1^0}$ plane for $\tilde{\tau}_1$ (stau-L) and $\tilde{\tau}_2$ (stau-R). The vertical dotted line indicates $\Delta m = m_{\tilde{\tau}_{1,2}} - m_{\tilde{\chi}_1^0} = m_\tau$, while the horizontal line indicates the detector-stable life time of 100 ns. The color coding is as in Fig. 1. Parameter points in agreement with all constraints, as shown in red, are found for all mass differences up to ~ 30 GeV.

For $\Delta m = m_{\tilde{\tau}_{1,2}} - m_{\tilde{\chi}_1^0} > m_\tau$, the staus decay promptly to $\tau\tilde{\chi}_1^0$ final state with very small lifetime $\lesssim 10^{-12}$ ns. For smaller mass gaps, $\Delta m \lesssim m_\tau$, three-body $(\to \pi\nu_\tau\tilde{\chi}_1^0)$ or four-body $(\to l\nu_l\nu_\tau\tilde{\chi}_1^0)$ final states dominate, which makes the stau lifetime longer, rendering them effectively detector-stable. It is apparent from Fig. 6 that the stau lifetimes in our scans lie orders of magnitude below the age of the universe $\sim 10^{17}$ s. This is in agreement with the non-observation of a heavy stable charged particle in DM search experiments. Moreover, a heavy stau of $\sim$ several hundred GeV, as obtained in our case, is expected to have sufficiently small number density so as not to hamper a successful big bang nucleosynthesis [220,222]. However, such long-lived staus might be subject to detector-stable particle searches at the LHC. We show in Fig. 7 our data sample in the plane $m_{\tilde{\tau}_{1,2}}$-$\tau_{\tilde{\tau}_{1,2}}$. The box shown indicates the parameter points that might be excluded by the current searches from ATLAS for stable charged particles, based on 36 fb^{-1} [187,188], reaching up to masses of $m_{\tilde{\tau}} \lesssim 430$ GeV. (CMS published a somewhat weaker limit based on ~ 13 fb^{-1} [223].) Since the ATLAS limits were obtained in a GMSB framework and the production cross section differs slightly from our calculation (see Sect. 5.5.1 below) we did not exclude these points from our data sample, but just indicate the points which may be affected by a gray region in Fig. 7. It should be noted that for the parameter points with the highest masses, $m_{\tilde{\tau}_{1,2}} \sim 550$ GeV, there are points with a short life time, as well as points which are detector-stable.

5.4 Prospects for DD experiments

We now turn to the prospects to cover the stau-L and stau-R scenario with DD experiments. In the upper (lower) plot of Fig. 8 we show the results of our scan in the stau-L (stau-R) case in the $m_{\tilde{\chi}_1^0}$–σ_p^{SI} plane, where σ_p^{SI} denotes the spin-independent DM scattering cross section (which are always substantially more relevant than the spin-dependent limits). The color coding of the points indicates the DM relic density, where the red points correspond to full agreement with the Planck measurement, see Eq. (4). For the points with a lower relic density we rescale the cross-section with a factor of $(\Omega_{\tilde{\chi}}h^2/0.118)$ to take into account the fact that $\tilde{\chi}_1^0$ pro-

---

[6] "Stable" should be seen as "detector-stable", corresponding to a lifetime of larger than ~ 100 ns.

[7] The additional decay modes included in Ref. [221] are expected to have only marginal effects in our lifetime values and no effect on our conclusion regarding the stable charged particle searches at the LHC.
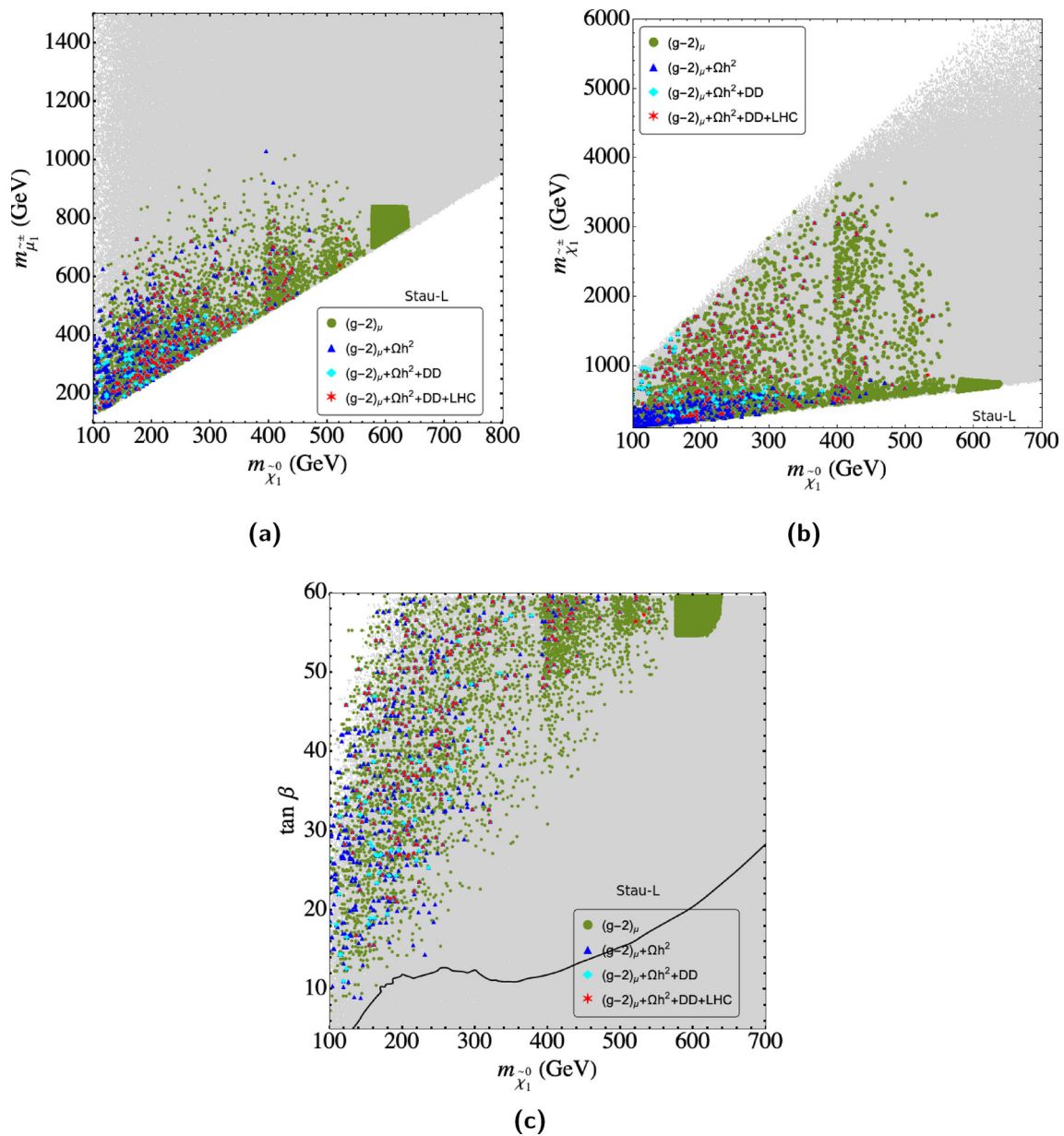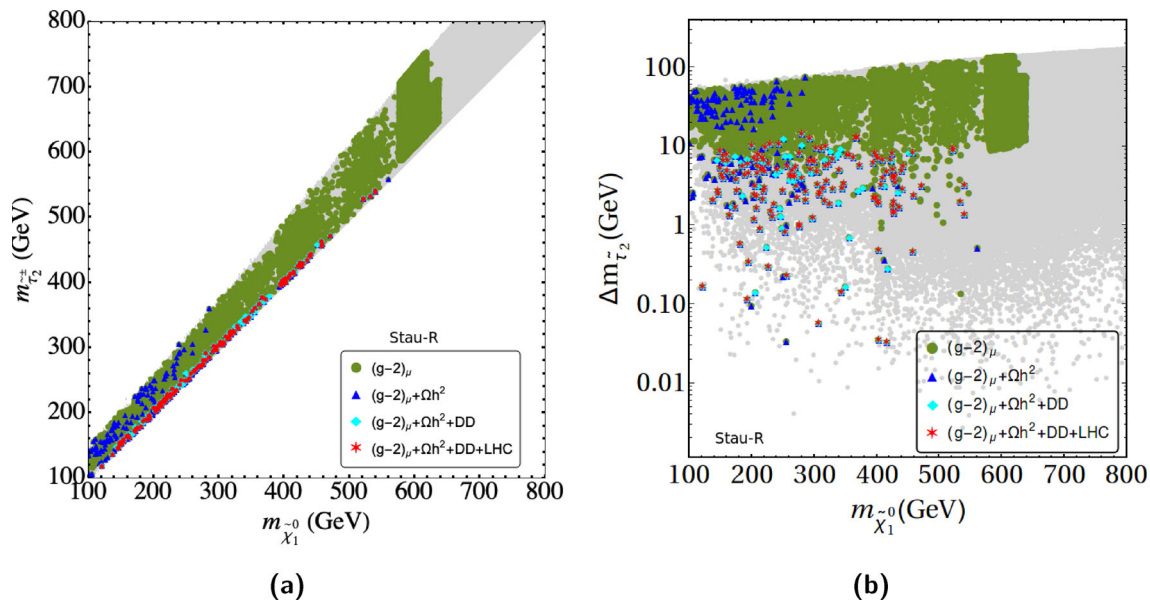
Fig. 3 The results of our parameter scan in the $\tilde{\tau}_1$-coannihilation case in the $m_{\tilde{\chi}_1^0}$–$m_{\tilde{\mu}_1}$ plane (top left), $m_{\tilde{\chi}_1^0}$–$m_{\tilde{\chi}_1^\pm}$ plane (top right) and $m_{\tilde{\chi}_1^0}$–$\tan\beta$ plane (bottom). For the color coding: see text

vides only a fraction of the total DM relic density of the universe. The various nearly horizontal lines indicate the reach of current and future DD experiments. The current bound is given in solid blue by LZ [196]. The future projection for LZ [224] and Xenon-nT [225] are shown as a black dashed line (which effectively agree with each other). Furthermore, we show the projection of the DarkSide [226] and the Argo [227]experiments, which can go down to even lower cross sections, as blue dashed and blue dot-dashed lines respectively. The lowest black, dot-dashed line indicates the neutrino floor [228]. Also shown for comparison is the previous "best" bound from Xenon-1T [111]. The results for the stau-

L and stau-R cases appear effectively identical and we will describe them together.

By construction, the upper limit of the points is provided by the latest LZ limit (solid blue line). The points of the scans appear nearly uniformly distributed. Also the red points, which represent the exact relic density appear nearly uniformly distributed. The allowed points go below the next round of Xenon based experiments as given by LZ/Xenon-nT, but also below the Argon based experiments, namely DarkSide and Argo. A substantial part of the allowed parameter space is even found below the neutrino floor. Interestingly, in both cases, stau-L and stau-R, a small population of

Fig. 4 The results of our parameter scan in the $\tilde{\tau}_2$-coannihilation case in the $m_{\tilde{\chi}_1^0}$–$m_{\tilde{\tau}_2}$ plane (left) and the $m_{\tilde{\chi}_1^0}$–$\Delta m_{\tilde{\tau}_2}$ plane ($\Delta m_{\tilde{\tau}_2} = m_{\tilde{\tau}_2} - m_{\tilde{\chi}_1^0}$, right plot). For the color coding: see text

points is found about one order of magnitude in σ_p^{SI} below the neutrino floor at masses above ~ 500 GeV. This is contrary to the findings for the five scenarios listed in Sect. 1, where all points found below the neutrino floor have $m_{\tilde{\chi}_1^0} \lesssim 500$ GeV [12]. For points below the neutrino floor the prospects to cover them in DD experiments are currently unclear. We will discuss the prospects to cover them at the HL-LHC and at future e^+e^- colliders, i.e. the complementarity of collider experiments and DD experiments, in the next subsections. It should be remembered that the points with masses larger than ~ 500 GeV can have a short life time, or can be detector-stable.

It should be noted here that we do not include here a discussion of indirect detection prospections, which would go beyond the scope of our paper. However, as we discussed in Ref. [12] that the indirect detection limits only play a relevant role in the case of higgsino DM.

5.5 Complementarity with future collider experiments

In this section we analyze the complementarity between future DD experiments and collider searches. We concentrate on the parameter points that are below the anticipated limits of LZ and XENON-nT, and in particular on the points below the neutrino floor. We first show the prospects for searches for EW SUSY particles at the approved HL-LHC [229]. Then we explore the prospects at possible future high-energy e^+e^- colliders, such as the ILC [230,231] or CLIC [231–234].

5.5.1 HL-LHC prospects

The prospects for BSM phenomenology at the HL-LHC, running at 14 TeV and collecting 3 ab^{-1} of integrated luminosity per detector, have been summarized in Ref. [229]. For the bino DM scenario with $\tilde{\tau}$-coannihilation, the searches that could be the most constraining are those looking for $\tilde{l}^{\pm}$-pair production (where one should distinguish between $\tilde{\tau}$-pair and $\tilde{e}+\tilde{\mu}$-pair production), as well as the $\tilde{\chi}_1^{\pm} - \tilde{\chi}_2^0$ production searches leading to three leptons and $\not{E}_T$ in the final state.[8] So far, to our knowledge, no projected sensitivity for the former search exists. Concerning the latter search, the projected 95% C.L. exclusion contours were provided by the ATLAS collaboration in Ref. [229] for the decays $\tilde{\chi}_1^{\pm}\tilde{\chi}_2^0 \rightarrow W^{\pm}Z$ and $\tilde{\chi}_1^{\pm}\tilde{\chi}_2^0 \rightarrow W^{\pm}h$. The corresponding limits are given for simplified model scenarios assuming $\tilde{\chi}_2^0$ and $\tilde{\chi}_1^{\pm}$ to be purely wino-like and mass-degenerate as well as $\tilde{\chi}_1^0$ to be purely bino-like. These searches are most effective in the regions with sufficiently large mass splitting: $\Delta m = m_{\tilde{\chi}_1^{\pm}} - m_{\tilde{\chi}_1^0} \gtrsim M_Z$ and $\Delta m \gtrsim M_h$ for the $W^{\pm}Z$ and $W^{\pm}h$ modes, respectively, where masses up to $m_{\tilde{\chi}_1^{\pm}} = m_{\tilde{\chi}_2^0} \sim 1.2$ TeV can be probed. The parameter region where $m_{\tilde{\chi}_1^{\pm}}, m_{\tilde{\chi}_2^0} > m_{\tilde{l}_L}, m_{\tilde{l}_R}$, the $\tilde{\chi}_1^{\pm}, \tilde{\chi}_2^0$ may also decay via sleptons of the first two generations, weakening the above bounds (the decay via staus, despite kinematically favored, leads to more complicated final states). The prospect for such decay channels, however has not been analyzed.

---

[8] $\tilde{\chi}_1^+(\rightarrow W^+\tilde{\chi}_1^0)\tilde{\chi}_1^-(\rightarrow W^-\tilde{\chi}_1^0)$ production leading to two leptons and $\not{E}_T$ in the final state usually gives rise to slightly weaker bounds.
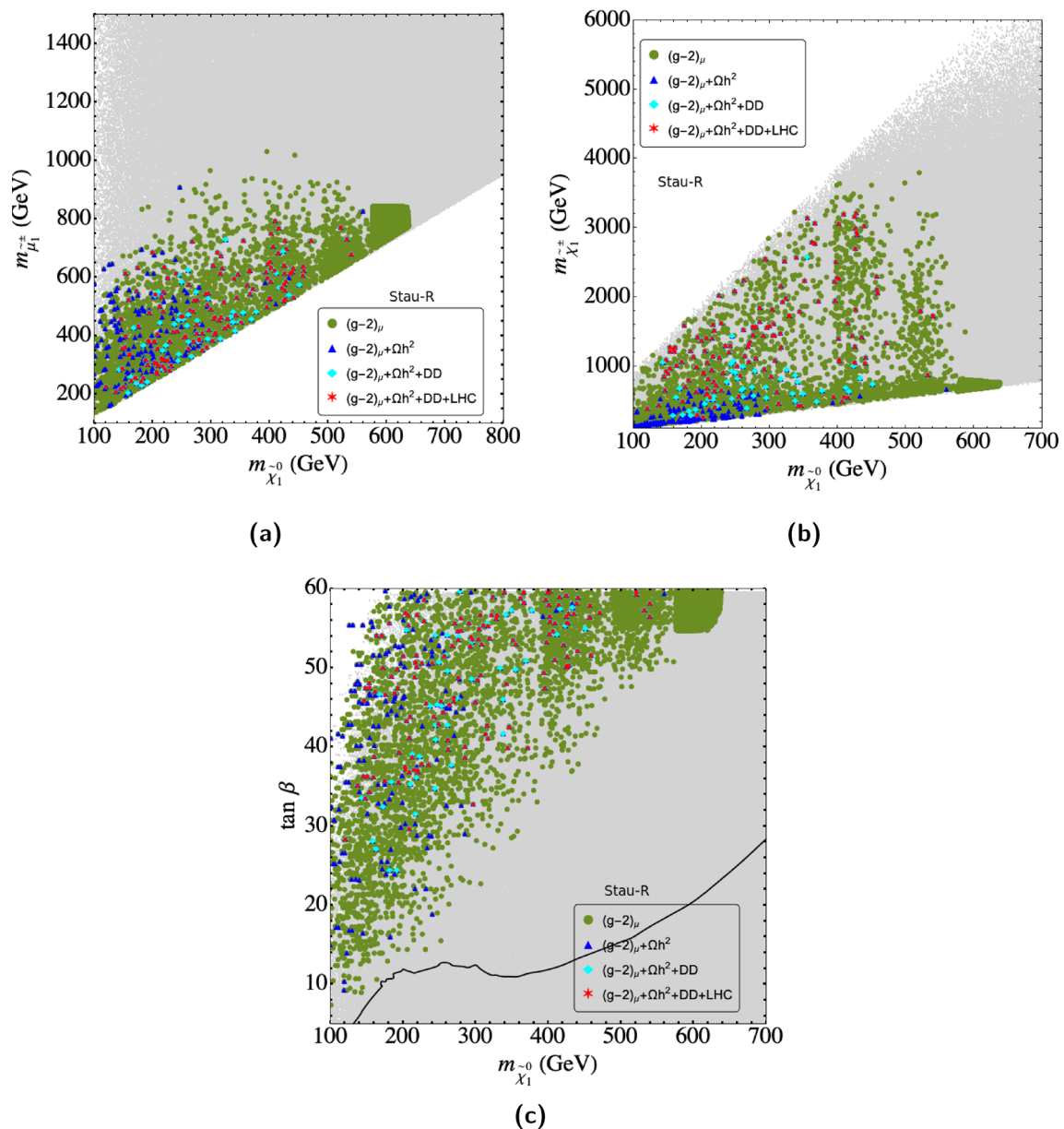
Fig. 5 The results of our parameter scan $\tilde{\tau}_2$-coannihilation case in the $m_{\tilde{\chi}_1^0}$–$m_{\tilde{\mu}_1}$ plane (top left), $m_{\tilde{\chi}_1^0}$–$m_{\tilde{\chi}_1^\pm}$ plane (top right) and $m_{\tilde{\chi}_1^0}$–$\tan\beta$ plane (bottom). For the color coding: see text

For stau pair production searches at the HL-LHC, the exclusion limit can reach 690 (430) GeV for pure $\tilde{\tau}_L$ ($\tilde{\tau}_R$) pair production, assuming a massless $\tilde{\chi}_1^0$ and a large ($\gtrsim 100$ GeV) mass difference between the stau and $\tilde{\chi}_1^0$ [229]. The discovery sensitivity for pure $\tilde{\tau}_L \tilde{\tau}_L$ production falls in the stau mass range $110 - 500$ GeV. However, no discovery sensitivity for pure $\tilde{\tau}_R \tilde{\tau}_R$ production could be obtained. This search may be applied to constrain the pair production of the heavier stau in our scenarios. Thus, at least a part of our parameter space may be probed by this search at the HL-LHC.

We calculated the NLO+NLL threshold resummed cross sections at the HL-LHC for $\tilde{\chi}_1^+ \tilde{\chi}_1^-$ and $\tilde{\chi}_1^+ \tilde{\chi}_2^0$ production

using the public package Resummino [235–239].[9] Despite the absence of clear future expected discovery/exclusion bounds for the slepton searches, in order to provide an estimate of the production cross section at the HL-LHC, we also computed the corresponding cross sections for $\tilde{e}_L^\pm \tilde{e}_L^\mp + \tilde{\mu}_L^\pm \tilde{\mu}_L^\mp$ productions, as well as for $\tilde{\tau}_{1/2}^\pm \tilde{\tau}_{1/2}^\mp$ production for the stau-L/R case.

In Fig. 9 we present our results for the relevant production cross sections in the stau-L scenario for the "surviving"

---

[9] We do not separately calculate $\tilde{\chi}_1^- \tilde{\chi}_1^0$ production cross section as it is expected to be very similar to that of $\tilde{\chi}_1^+ \tilde{\chi}_2^0$.
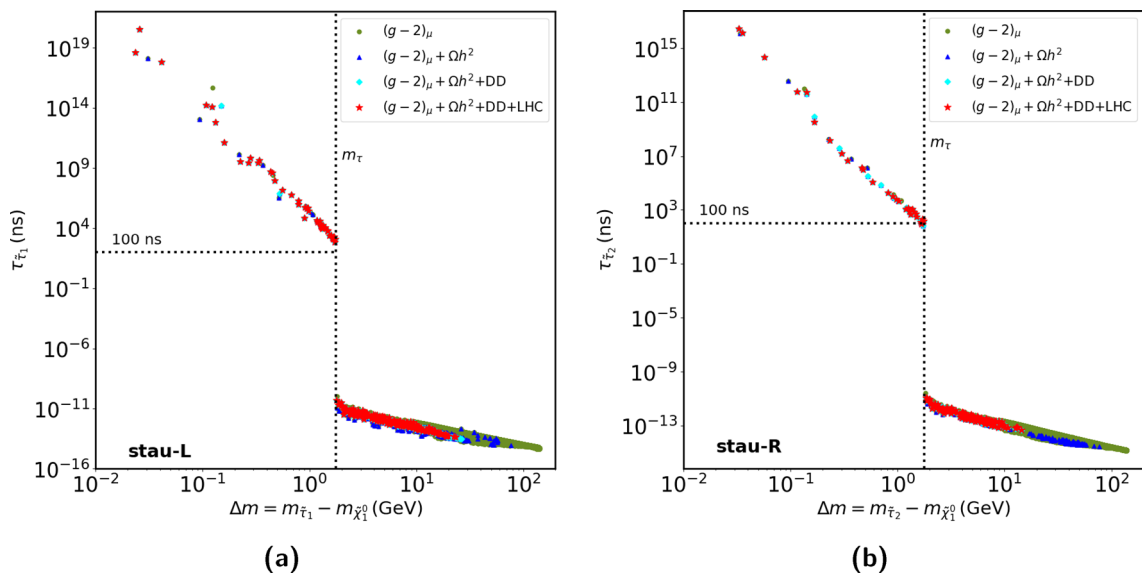
Fig. 6 Lifetime as a function of mass difference $\Delta m = m_{\tilde{\tau}_{1,2}} - m_{\tilde{\chi}_1^0}$ for $\tilde{\tau}_1$ in case-L (left) and $\tilde{\tau}_2$ in case-R (right). The color coding is as in Fig. 1
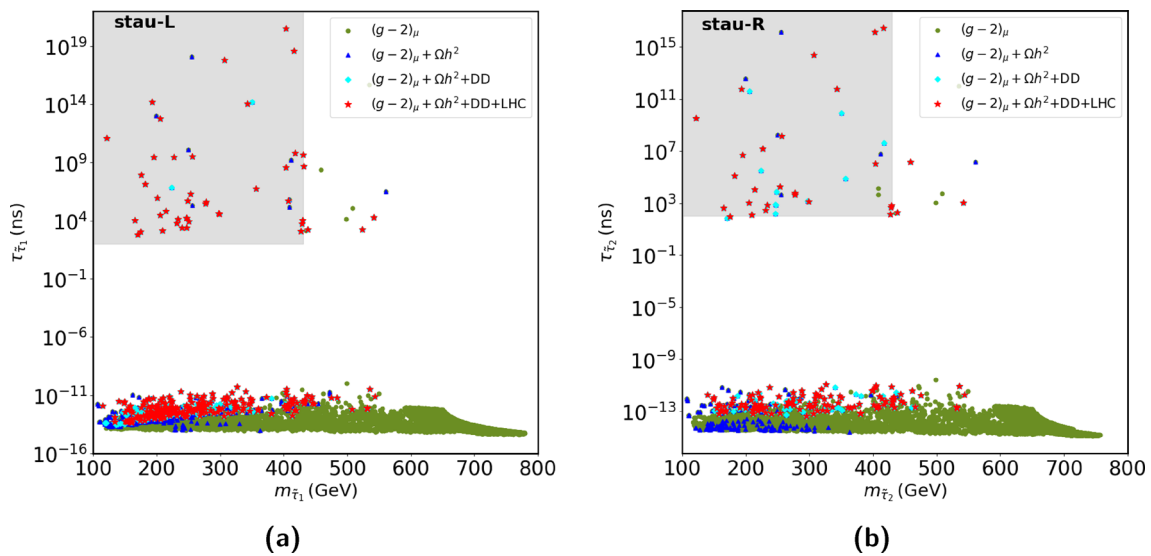

Fig. 7 Lifetime as a function of mass for $\tilde{\tau}_1$ in case-L (left) and $\tilde{\tau}_2$ in case-R (right). The color coding is as in Fig. 1

points, i.e. the parameter points passing all constraints. In the upper row we show $\sigma(pp \to \tilde{\tau}_1\tilde{\tau}_1)$ as a function of $m_{\tilde{\tau}_1}$ (left) and $\Delta m_{\tilde{\tau}_1} = m_{\tilde{\tau}_1} - m_{\tilde{\chi}_1^0}$ (right). In the lower row we show $\sigma(pp \to \tilde{e}_L\tilde{e}_L + \tilde{\mu}_L\tilde{\mu}_L)$ (left) and $\sigma(pp \to \tilde{\chi}_1^+\tilde{\chi}_1^-, \tilde{\chi}_1^+\tilde{\chi}_2^0)$ (right). In the upper and lower left plots the green and blue stars represent points below the sensitivity of Xenon-nT/LZ and the neutrino floor, respectively. In the lower right plot the orange and green squares show the results for $\tilde{\chi}_1^+\tilde{\chi}_1^-$ and $\tilde{\chi}_1^+\tilde{\chi}_2^0$ production for points below the Xenon-nT/LZ sensitivity, whereas the blue and black stars indicate the corresponding results for points below the neutrino floor.

We start our discussion of the HL-LHC prospects in the stau-L scenario with $\tilde{\tau}_1$ pair production, as presented in the

upper row of Fig. 9. Here it should be kept in mind that these events are characterized by compressed spectra and thus soft taus, see the discussion in Sect. 5.3. Concerning the numerical results, due to phase space, the pair production cross section goes down with $m_{\tilde{\tau}_1}$, starting at 50 fb at $m_{\tilde{\tau}_1} \lesssim 200$ GeV, going down below 0.5 fb for the points with $m_{\tilde{\tau}_1} \sim 550$ GeV (see the discussion in the previous subsection). The latter results in less than 1500 events in each LHC experiment, and the discovery prospects are unclear, particularly due to the compressed spectra. For the previously discussed searches for stable charged particles [187,188,223] no projection for the HL-LHC is available. However, it is conceivable that the current limits of $m_{\tilde{\tau}} \gtrsim 430$ GeV can be
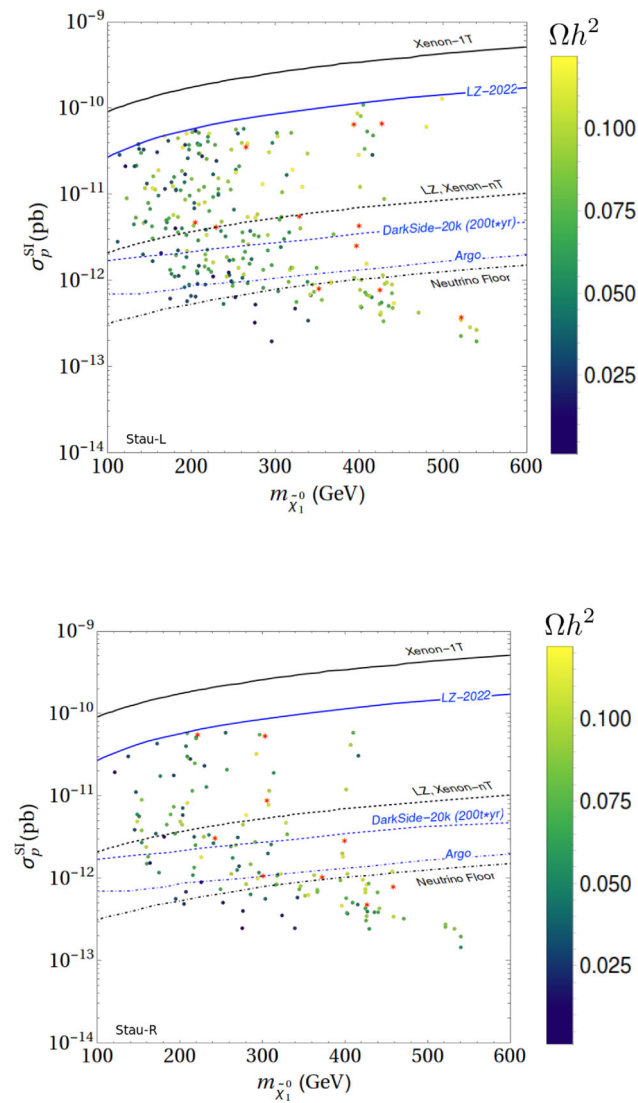
Fig. 8 Surviving points $m_{\tilde{\chi}_1^0}$–σ_p^{SI} plane for stau-L (upper plot) and stau-R (lower plot) case. The color coding indicates the relic abundance, where red points denote the points with correct relic abundance. The various nearly horizontal lines indicate the reach of current and future DD experiments (see text). The lowest black dot-dashed line shows the neutrino floor

extended up to ~ 550 GeV with the large data sets expected from the HL-LHC. These may exclude some of the points with $m_{\tilde{\tau}_1} \sim 550$ GeV, but not all of them, as a subset of them has a far too short life time. As a general (but not strict) trend one observes that larger masses are correlated with smaller σ_p^{SI}, such that the highest mass points are all below the neutrino floor. Consequently, for the highest mass points both DD experiments as well as the HL-LHC do not seem to offer the possibility to experimentally test these scenarios.

Next, in the lower left plot the cross section for slepton-pair production of the first two generations is presented. The experimental situation should be better than for $\tilde{\tau}_1$-pair pro-

duction due to the non-compressed spectra and the fact that muons and electrons are experimentally easier accessible than taus. As discussed in Sect. 5.1, now the masses range for ~ 300 to ~ 800 GeV. As before, the phase space leads to smaller cross sections for larger masses, where for equal $\tilde{\mu}_L/\tilde{e}_L$ and $\tilde{\tau}_1$ masses roughly a factor of ~ 2 reduction between the two production cross sections can be observed, owing to the sum of the first and second generation sleptons. For the largest masses now ~ 0.1 fb are found, resulting in ~ 300 events, leaving the discovery prospects very unclear.

The last cross sections discussed in the stau-L scenario are the ones for charginos and neutralinos as shown in the lower right plot of Fig. 9. The two shown cross sections, $\tilde{\chi}_1^+ \tilde{\chi}_1^\mp$ and $\tilde{\chi}_1^+ \tilde{\chi}_2^0$ yield effectively the same results and are thus described together. Naturally, due do phase space the lowest masses yield the largest cross sections, where chargino/neutralino masses around ~ 400 GeV can reach a production cross section of ~ 1 pb. However, the apparently large cross section reached for relatively light masses has to be interpreted with caution in deriving future exclusion/discovery potentials: on the one hand, $\tilde{\chi}_1^+$, $\tilde{\chi}_2^0$ and $\tilde{\chi}_1^+ \tilde{\chi}_1^-$ may decay partly via sleptons of the first two generations, weakening the limits from gauge-boson or Higgs-mediated decays. On the other hand, they may decay to some extent via $\tilde{\tau}$'s, relaxing the bounds from both slepton-mediated and gauge/Higgs-boson mediated decays. Even more complicated are some points below the neutrino floor, which are found with masses between 2.5 TeV and 3 TeV. From Fig. 3 one can see that these points coincide with the largest $m_{\tilde{\chi}_1^0}$ values. These have production cross sections at the level of $\sim 10^{-5}$ fb, which are clearly beyond the reach of the HL-LHC.

We now turn to the $\tilde{\tau}_2$-pair, first and second generation slepton-pair production, as well to the production of $\tilde{\chi}_1^+ \tilde{\chi}_2^0$ and $\tilde{\chi}_1^+ \tilde{\chi}_1^-$ in the stau-R scenario. Our results are presented in Fig. 10 with the same order of plots and the same color coding as in Fig. 9. The results turn out effectively identical to the stau-L case. Small differences in the various production cross sections can be observed, but they do not play any relevant phenomenological role. Consequently, we refrain from a detailed discussion of these EW production cross sections. However, it is important to note that also in the stau-R case, points with $m_{\tilde{\chi}_1^0} \sim 550$ GeV are found that are below the neutrino floor These points with $\tilde{\tau}_2$-pair production cross sections of ~ 0.5 fb (where only a subset may be tested with stable charged particle searches at the HL-LHC), first plus second generation slepton production cross section of ~ 0.1 fb and chargino/neutralino cross sections of $\sim 10^{-4}$ fb, are likely to escape the searches at the HL-LHC.

In summary, taking into account the DD limits and the EW production cross sections and the stable charged particle searches discussed in this section, the complementarity
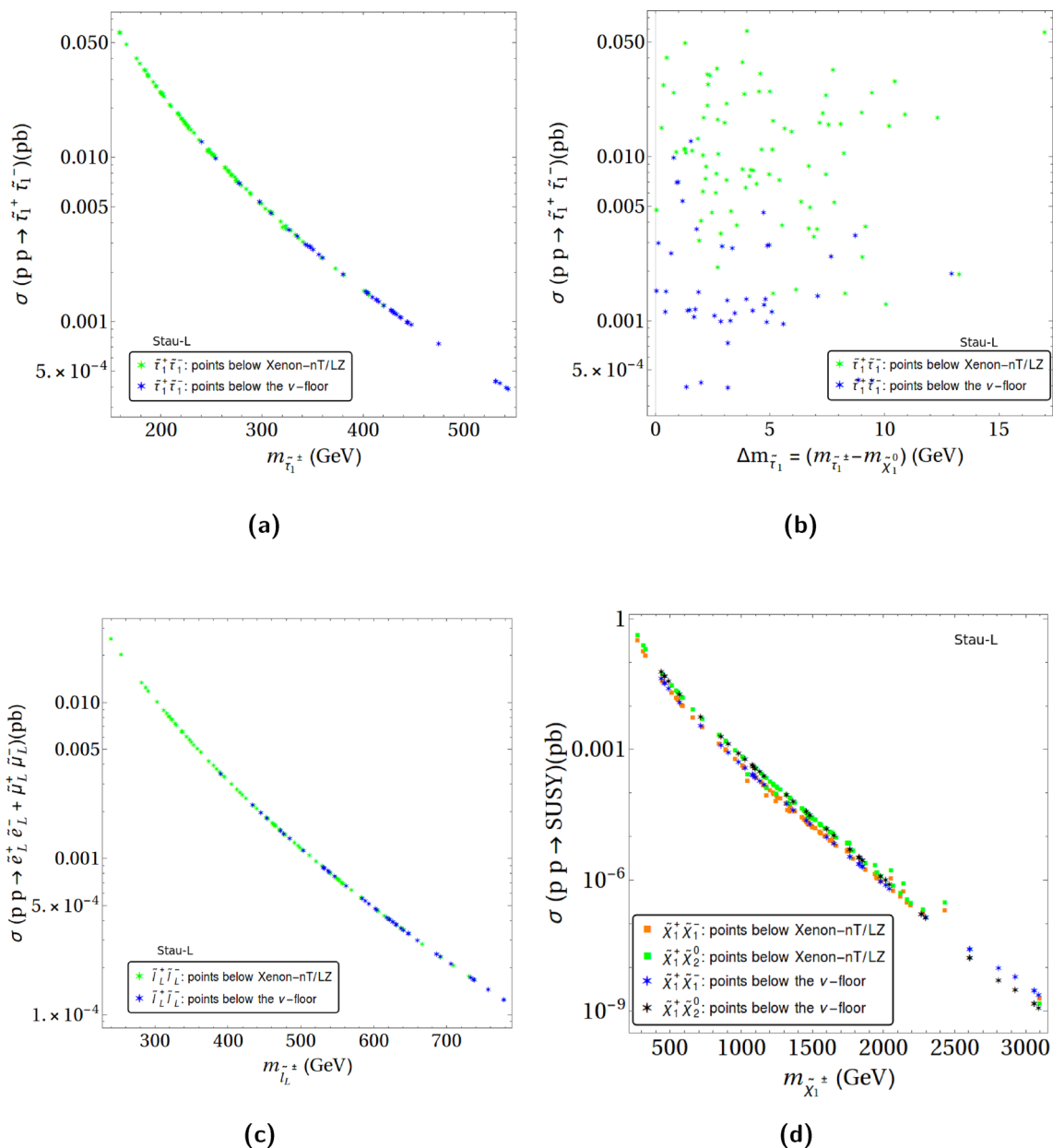
(a)

(b)

(c)

(d)

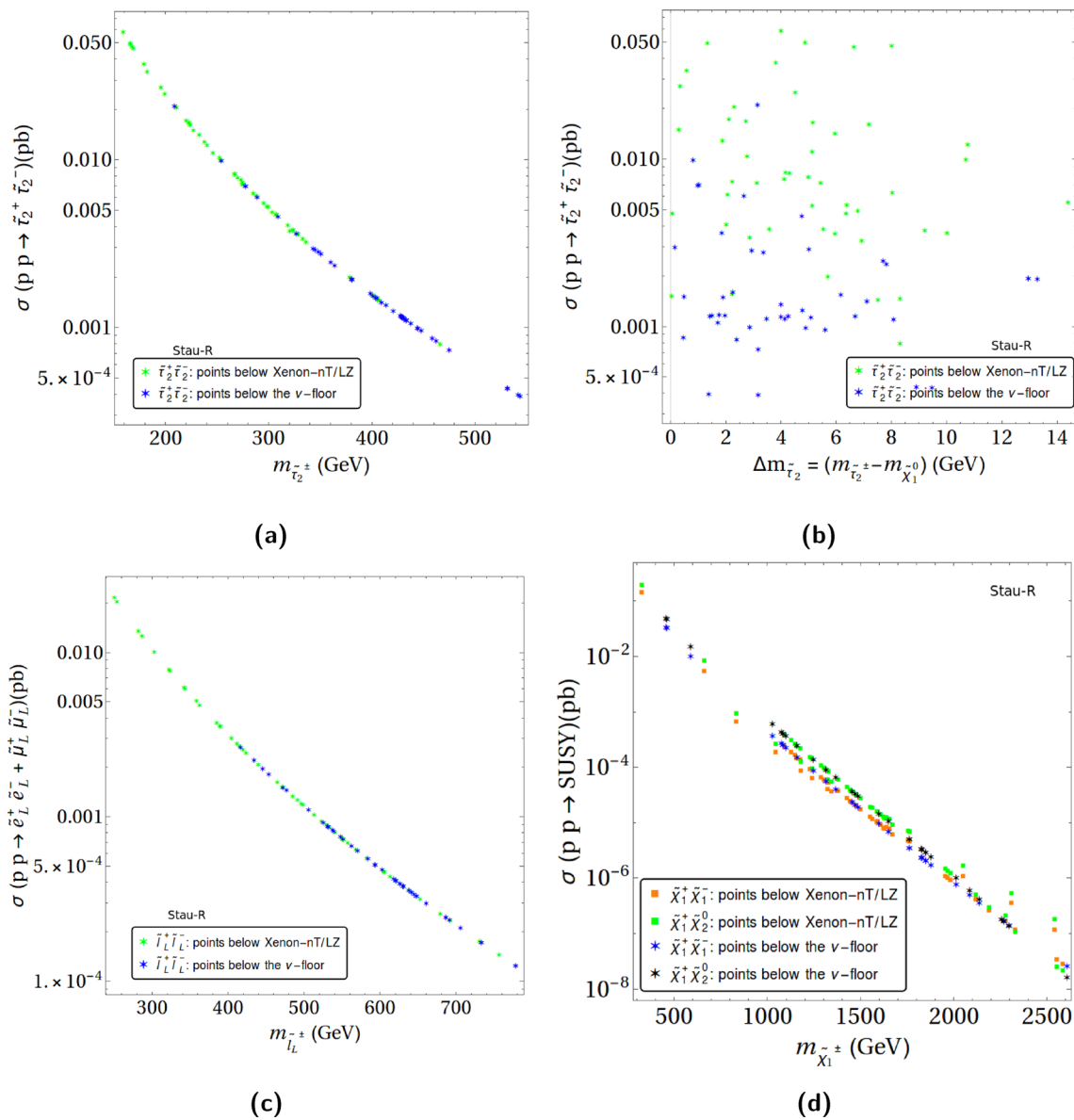**Fig. 9** The cross-sections of the surviving parameter points in the stau-L scenario. Upper row: $\sigma(pp \to \tilde{\tau}_1 \tilde{\tau}_1)$ as a function of $m_{\tilde{\tau}_1}$ (left) and $\Delta m_{\tilde{\tau}_1} = m_{\tilde{\tau}_1} - m_{\tilde{\chi}_1^0}$ (right). Lower row: $\sigma(pp \to \tilde{e}_L \tilde{e}_L + \tilde{\mu}_L \tilde{\mu}_L)$ (left) and $\sigma(pp \to \tilde{\chi}_1^+ \tilde{\chi}_1^-, \tilde{\chi}_1^+ \tilde{\chi}_2^0)$ (right). For the color coding: see text

between the DD experiments and the HL-LHC can not conclusively be answered: some points of the stau-L and stau-R scenarios could escape both types of experiments.

5.5.2 ILC/CLIC prospects

The direct production of EW particles at e^+e^- colliders requires a sufficiently high center-of-mass energy, $\sqrt{s}$ that can only be reached at linear e^+e^- colliders, such as ILC [230,231] and CLIC [231–234]. Those colliders can reach energies up to 1 TeV, and 3 TeV, respectively. Here we focus

on the the final energy stage of the ILC, also denoted as ILC1000.

We evaluate the cross-sections for LSP and NLSP production modes for $\sqrt{s} = 1$ TeV, which can be reached at the ILC1000. We note here that with the anticipated higher energies at the CLIC, larger production cross section and higher mass reach is expected. At the ILC1000 an integrated luminosity of 8 ab^{-1} is foreseen [240,241]. Our cross-section predictions[10] are based on tree-level results, obtained as

---

Fig. 10 The cross-sections of the surviving parameter points in the stau-R scenario. Upper row: $\sigma(pp \to \tilde{\tau}_2\tilde{\tau}_2)$ as a function of $m_{\tilde{\tau}_2}$ (left) and $\Delta m_{\tilde{\tau}_2} = m_{\tilde{\tau}_2} - m_{\tilde{\chi}_1^0}$ (right). Lower row: $\sigma(pp \to \tilde{e}_L\tilde{e}_L + \tilde{\mu}_L\tilde{\mu}_L)$ (left) and $\sigma(pp \to \tilde{\chi}_1^+\tilde{\chi}_1^-, \tilde{\chi}_1^+\tilde{\chi}_2^0)$ (right). For the color coding: see text

in Refs. [242,243]. In those articles it was shown that the full one-loop corrections to our production cross sections can amount up to 10–20%.[11] Here we do not attempt a rigorous experimental analysis, but rather follow the analyses in Refs. [245–247] that indicate that to a good approximation final states with the sum of the masses smaller than the center-of-mass energy can be detected.

In Fig. 11 we present the LSP and NLSP pair production cross sections for an e^+e^- collider at $\sqrt{s} = 1000$ GeV as a function of the two (identical) final state masses. In the left and right plots the results for the stau-L and stau-R scenario, respectively, are shown. In each plot we show $\sigma(e^+e^- \to \tilde{\chi}_1^0\tilde{\chi}_1^0(+\gamma))$ production[12] in green, and $\sigma(e^+e^- \to \tilde{\tau}_1\tilde{\tau}_1)$ ($\sigma(e^+e^- \to \tilde{\tau}_2\tilde{\tau}_2)$) in violet in the left (right) plot of Fig. 11.

The open circles denote the points below the anticipated XENON-nT/LZ limit, whereas the solid circles correspond to

---

[11] Including the full one-loop corrections here as done in Refs. [242, 243] would have required to determine the preferred renormalization scheme for each point individually (see Refs. [119,120,244] for details), which goes beyond the scope of this analysis.

---

[12] Our tree level calculation does not include the photon radiation, which appears only starting from the one-loop level. However, such an ISR photon is crucial to detect this process due to the invisible final state. We take our tree-level cross section as a rough approximation of the cross section including the ISR photon, see also Ref. [242] and use the notation "$(+\gamma)$".
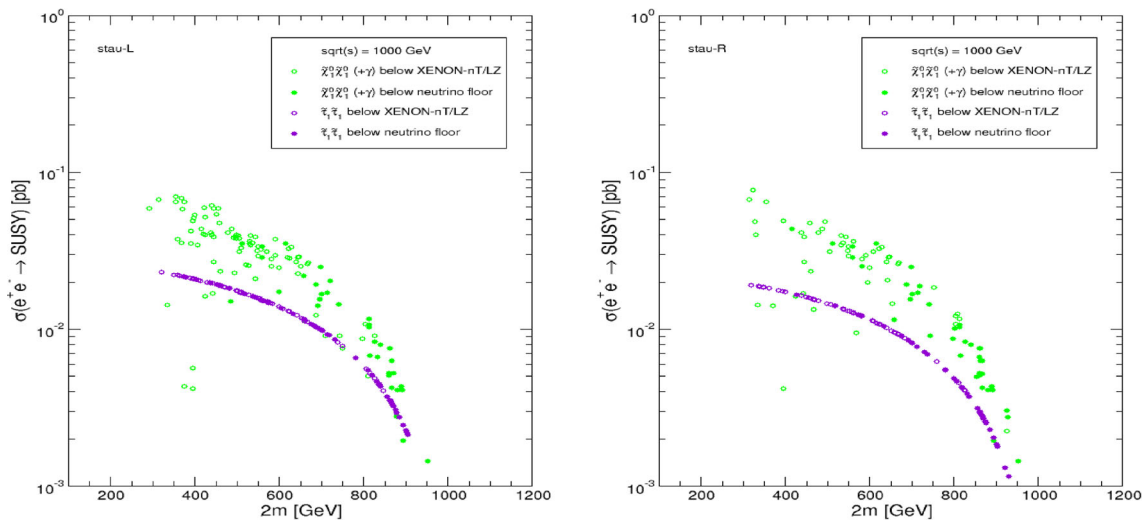
Fig. 11 Cross section predictions at an e^+e^- collider with $\sqrt{s} = 1000$ GeV as a function of the sum of two final state masses. left plot: $\tilde{\tau}_1$-coannihilation (stau-L); right plot: $\tilde{\tau}_2$-coannihilation (stau-R). The color code indicates the final state, open circles are below the anticipated Xenon-nT/LZ reach, full circles are below the neutrino floor

the points below the neutrino floor. The cross sections range roughly from ~ 50 fb for low masses to ~ 1 fb for the largest masses shown in the plots, reaching nearly the kinematic limit of the ILC1000, i.e. $m_{\tilde{\chi}_1^0} \lesssim 500$ GeV (and the stau masses accordingly). Assuming an integrated luminosity of 8 ab^{-1}, this corresponds to $\sim 8000 - 400{,}000$ events. Consequently, the ILC should be able to detect SUSY particles in all cases with masses just below 500 GeV. However, here it is important to note that in both scenarios, stau-L and stau-R, a group of points are found in the range of $m_{\tilde{\chi}_1^0} \sim 550$ GeV, with the stau masses very slightly above (where only a subset of them may be tested with stable charged particle searches at the HL-LHC). In order to cover these points a slightly higher center-of-mass energy up to $\sqrt{s} \sim 1100$ GeV would be necessary. (A second stage CLIC with $\sqrt{s} \sim 1500$ GeV would clearly be sufficient to cover the two scenarios.)

These results are in contrast to the other five cases analyzed previously in Ref. [12]. In these cases, and in particular for $\tilde{l}^{\pm}$-coannihilation with all three slepton generations having degenerate soft SUSY-breaking terms, the DD experiments together with the ILC1000 could cover all parameter points. Allowing for a non-degeneracy between staus and first/second generation sleptons leads to slightly higher masses that can accommodate all constraints, thus avoiding the detectability at the ILC1000.

6 Conclusions

We performed an analysis of the EW sector of the MSSM featuring stau-coannihilation, taking into account all the latest relevant experimental and theoretical constraints. The experimental results comprised the current DM relic abundance (either as an upper limit or as a direct measurement), the DM direct detection (DD) experiments, the direct searches at the LHC, and in particular the deviation of the anomalous magnetic moment of the muon [164].

In our previous works, five different scenarios were analyzed [9–12], classified by the mechanism that brings the LSP relic density into agreement with the measured values. The scenarios differ by the nature of the Next-to-LSP (NLSP), or equivalently by the mass hierarchies between the mass scales determining the neutralino, chargino and slepton masses. In all scenarios a degeneracy between the three generations of sleptons was assumed, motivated by simplicity of the analysis as well as keeping in mind the degeneracy solution to the SUSY flavour problem. This becomes particularly relevant for $\tilde{l}^{\pm}$-coannihilation where the degeneracy results in a direct connection between the masses of the smuons involved in the explanation for $(g-2)_\mu$ to that of the NLSP which acts as a coannihilation partner to the LSP in explaining the DM content of the universe. On the other hand, in well-motivated top-down models such as mSUGRA, such degeneracy does not exist in general and often the lighter stau becomes the NLSP at the EW scale via renormalization group running, with the smuons/selectron masses lying slightly above. Consequently, a full mass degeneracy of the three slepton families should be regarded as an artificial constraint, which may lead to artefacts in the phenomenological analysis [129,130].

In this paper we analyzed an MSSM scenario at the EW scale, assuming degeneracy only between smuons and selectrons, but non-degeneracy of the staus, and enforcing stau coannihilation. We required either the left- or the right-

handed mass parameter to be close to M_1 (labelled stau-L and stau-R scenarios, respectively). For these two scenarios, corresponding more to a top-down model motivated mass hierarchy we analyzed the viable parameter space, taking into account all relevant theoretical and experimental constraints. In both scenarios we find upper limits of $m_{\tilde{\chi}_1^0} \lesssim 550$ GeV with a very small mass difference between the neutralino LSP and the stau NLSP.

We have paid particular attention to the NLSP life time, as the mass difference between the $\tilde{\chi}_1^0$ and the lighter $\tilde{\tau}$ can be as low as $\mathcal{O}(10$ MeV). Parameter points with a mass difference lower than m_τ yield effectively detector-stable staus, which could be subject to current searches for long lived charged particles. The current bounds for particles with a life time larger than ~ 100 ns reach up to $m_{\tilde{\tau}} \lesssim 430$ GeV and can potentially exclude part of these points. It is conceivable that the current limits can be extended up to ~ 550 GeV with the large data sets expected from the HL-LHC. However, some points with stau masses of ~ 550 GeV have a larger mass difference and thus a far too short life time to be affected by these searches.

In the second step we evaluated the prospects for future DD experiments to probe the two scenarios, where we showed explicitly the anticipated reach of XENON-nT, LZ, DarkSide and Argo. XENON-nT and LZ have a similar reach, which is moderately improved by DarkSide and a little further by Argo. For our two cases, stau-L and stau-R, the allowed points with the correct relic abundance can be found not only above, but also below the projected reach of XENON-nT/LZ and the Argon based experiments. The parameter points with the lowest DD cross section are the ones with the larges $\tilde{\chi}_1^0$ mass, nearly mass degenerate with the respective scalar tau. These points have a DD cross section below the neutrino floor and thus cannot be tested in with current DD technologies.

In continuation, we show that the HL-LHC and the ILC1000 (the e^+e^- ILC operating at an energy of up to 1000 GeV) can play complementary roles to probe the parameter space obtained below the anticipated XENON-nT/LZ limit or even below the neutrino floor. For the HL-LHC we evaluated the production cross sections of the NLSPs, the first/second generation of sleptons, as well as the $\tilde{\chi}_1^\pm$ and $\tilde{\chi}_2^0$. The largest cross sections are found for sleptons, ranging from ~ 10 fb for the smallest masses to ~ 0.1 fb for the largest masses. Here it must be kept in mind that the lighter stau is close in mass with the $\tilde{\chi}_1^0$, making their observation at the HL-LHC extremely difficult (as also discussed for the finite stau life time above). The largest allowed stau masses, corresponding to small mass differences will thus not be detectable at the HL-LHC (where only part of these points may be testable with the stable charged particle searches at the HL-LHC). Similarly, with a production cross section of ~ 0.1 fb for smuon/selectron production, also these EW particles will remain elusive at the HL-LHC.

The production cross sections for charginos and neutralinos are found to be even smaller, where the largest $\tilde{\chi}_1^0$ masses correspond to very large values of $m_{\tilde{\chi}_2^0}$ and $m_{\tilde{\chi}_1^\pm}$. Consequently, also these searches will not be able to cover these parameter points.

The situation is substantially better at the ILC1000. It is known in general that e^+e^- colliders can probe mass spectra with very small mass splittings. Consequently, one does not have to rely on the production of heavier SUSY particles, but can study the production of the LSP (with an ISR photon) and the stau NLSP. We have calculated the corresponding production cross sections for all points below the XENON-nT/LZ limit or the neutrino floor. All points within the kinematic reach have SUSY production cross sections above ~ 1 fb and can thus be detected at the ILC1000. However, as discussed above, in both scenarios, stau-L and stau-R, a group of points was found in the range of $m_{\tilde{\chi}_1^0} \sim 550$ GeV, with the stau masses very slightly above. In order to cover these points a slightly higher center-of-mass energy up to $\sqrt{s} \sim 1100$ GeV would be necessary. (A second stage CLIC with $\sqrt{s} \sim 1500$ GeV would clearly be sufficient to cover the two scenarios.) These results are in contrast to the other five cases analyzed previously in Ref. [12], where the combination of DD experiments and the ILC1000 covered *all* points below the projected Xenon-nT/LZ limits (and thus below the neutrino floor). The the case of $\tilde{\tau}$-coannihilation, i.e. allowing for a non-degeneracy between staus and first/second generation sleptons leads to slightly higher masses that can accommodate all constraints, thus avoiding the detectability at the ILC1000.

Note added

While we were finalizing our results, the "MUON G-2" collaboration published their results from Run 2 and 3 [248]. The value of $(g-2)_\mu$ of these runs

$$a_\mu^{\text{Run2,3}} = (11659205.5 \pm 2.4) \times 10^{-10} . \tag{8}$$

is well compatible with the previous results from Run 1, as well as with the (so far) world average. The new combined value of

$$a_\mu^{\text{exp-new}} = (11659205.9 \pm 2.2) \times 10^{-10} . \tag{9}$$

compared with the SM prediction in Eq. (1), yields a deviation of

$$\Delta a_\mu = (24.9 \pm 4.8) \times 10^{-10} , \tag{10}$$

corresponding to a 5.1σ discrepancy. While this new results will mildly shrink the parameter ranges allowed by $(g-2)_\mu$,

the overall conclusions of the paper concerning the combined upper limits on the (N)LSP masses and future prospects remain unchanged.

Data Availability Statement This manuscript has no associated data or the data will not be deposited. [Authors' comment: The relevant data is already included in the paper.]

References

1. H. Nilles, Phys. Rep. **110**, 1 (1984)
2. R. Barbieri, Riv. Nuovo Cim. **11**, 1 (1988)
3. H. Haber, G. Kane, Phys. Rep. **117**, 75 (1985)
4. J. Gunion, H. Haber, Nucl. Phys. B **272**, 1 (1986)
5. S. Heinemeyer, C. Muñoz, Universe **8**(8), 427 (2022)
6. H. Goldberg, Phys. Rev. Lett. **50**, 1419 (1983)
7. J. Ellis, J. Hagelin, D. Nanopoulos, K. Olive, M. Srednicki, Nucl. Phys. B **238**, 453 (1984)
8. K.J. Bae, H. Baer, E.J. Chun, Phys. Rev. D **89**(3), 031701 (2014). arXiv:1309.0519 [hep-ph]
9. M. Chakraborti, S. Heinemeyer, I. Saha, Eur. Phys. J. C **80**(10), 984 (2020). arXiv:2006.15157 [hep-ph]
10. M. Chakraborti, S. Heinemeyer, I. Saha, Eur. Phys. J. C **81**(12), 1069 (2021). arXiv:2103.13403 [hep-ph]
11. M. Chakraborti, S. Heinemeyer, I. Saha, Eur. Phys. J. C **81**(12), 1114 (2021). arXiv:2104.03287 [hep-ph]
12. M. Chakraborti, S. Heinemeyer, I. Saha, C. Schappacher, Eur. Phys. J C **82**(5), 483 (2022). arXiv:2112.01389 [hep-ph]
13. E. Bagnaschi, M. Chakraborti, S. Heinemeyer, I. Saha, G. Weiglein, Eur. Phys. J C **82**(5), 474 (2022). arXiv:2203.15710 [hep-ph]
14. M. Endo, K. Hamaguchi, S. Iwamoto, T. Kitahara, JHEP **07**, 075 (2021). arXiv:2104.03217 [hep-ph]
15. S. Iwamoto, T.T. Yanagida, N. Yokozaki, Phys. Lett. B **823**, 136768 (2021). arXiv:2104.03223 [hep-ph]
16. Y. Gu, N. Liu, L. Su, D. Wang, Nucl. Phys. B **969**, 115481 (2021). arXiv:2104.03239 [hep-ph]
17. M. Van Beekveld, W. Beenakker, M. Schutten, J. De Wit, SciPost Phys. **11**(3), 049 (2021). arXiv:2104.03245 [hep-ph]
18. W. Yin, JHEP **06**, 029 (2021). arXiv:2104.03259 [hep-ph]
19. F. Wang, L. Wu, Y. Xiao, J.M. Yang, Y. Zhang, Nucl. Phys. B **970**, 115486 (2021). arXiv:2104.03262 [hep-ph]
20. M. Abdughani, Y.Z. Fan, L. Feng, Y.L. Sming Tsai, L. Wu, Q. Yuan, Sci. Bull. **66**, 2170–2174 (2021). arXiv:2104.03274 [hep-ph]
21. J. Cao, J. Lian, Y. Pan, D. Zhang, P. Zhu, JHEP **09**, 175 (2021). arXiv:2104.03284 [hep-ph]
22. M. Ibe, S. Kobayashi, Y. Nakayama, S. Shirai. arXiv:2104.03289 [hep-ph]
23. P. Cox, C. Han, T.T. Yanagida, Phys. Rev. D **104**(7), 075035 (2021). arXiv:2104.03290 [hep-ph]
24. C. Han. arXiv:2104.03292 [hep-ph]
25. S. Heinemeyer, E. Kpatcha, I. Lara, D.E. López-Fogliani, C. Muñoz, N. Nagata, Eur. Phys. J. C **81**(9), 802 (2021). arXiv:2104.03294 [hep-ph]
26. S. Baum, M. Carena, N.R. Shah, C.E.M. Wagner. arXiv:2104.03302 [hep-ph]
27. H.B. Zhang, C.X. Liu, J.L. Yang, T.F. Feng. arXiv:2104.03489 [hep-ph]
28. W. Ahmed, I. Khan, J. Li, T. Li, S. Raza, W. Zhang. arXiv:2104.03491 [hep-ph]
29. P. Athron, C. Balázs, D.H. Jacob, W. Kotlarski, D. Stöckinger, H. Stöckinger-Kim, JHEP **09**, 080 (2021). arXiv:2104.03691 [hep-ph]
30. A. Aboubrahim, M. Klasen, P. Nath, Phys. Rev. D **104**(3), 035039 (2021). arXiv:2104.03839 [hep-ph]
31. M. Chakraborti, L. Roszkowski, S. Trojanowski, JHEP **05**, 252 (2021). arXiv:2104.04458 [hep-ph]
32. H. Baer, V. Barger, H. Serce, Phys. Lett. B **820**, 136480 (2021). arXiv:2104.07597 [hep-ph]
33. W. Altmannshofer, S.A. Gadam, S. Gori, N. Hamer. arXiv:2104.08293 [hep-ph]
34. M. Chakraborti, S. Heinemeyer, I. Saha. arXiv:2105.06408 [hep-ph]
35. M.D. Zheng, H.H. Zhang. arXiv:2105.06954 [hep-ph]
36. K.S. Jeong, J. Kawamura, C.B. Park, JHEP **10**, 064 (2021). arXiv:2106.04238 [hep-ph]
37. Z. Li, G.L. Liu, F. Wang, J.M. Yang, Y. Zhang. arXiv:2106.04466 [hep-ph]
38. P.S.B. Dev, A. Soni, F. Xu. arXiv:2106.15647 [hep-ph]
39. J.S. Kim, D.E. Lopez-Fogliani, A.D. Perez, R.R. de Austri. arXiv:2107.02285 [hep-ph]
40. J. Ellis, J.L. Evans, N. Nagata, D.V. Nanopoulos, K.A. Olive. arXiv:2107.03025 [hep-ph]
41. S.M. Zhao, L.H. Su, X.X. Dong, T.T. Wang, T.F. Feng. arXiv:2107.03571 [hep-ph]
42. M. Frank, Y. Hiçyılmaz, S. Mondal, Ö. Özdal, C.S. Ün, JHEP **10**, 063 (2021). arXiv:2107.04116 [hep-ph]
43. Q. Shafi, C.S. Un. arXiv:2107.04563 [hep-ph]
44. S. Li, Y. Xiao, J.M. Yang. arXiv:2107.04962 [hep-ph]
45. A. Aranda, F.J. de Anda, A.P. Morais, R. Pasechnik. arXiv:2107.05495 [hep-ph]
46. A. Aboubrahim, M. Klasen, P. Nath, R.M. Syed. arXiv:2107.06021 [hep-ph]
47. Y. Nakai, M. Reece, M. Suzuki, JHEP **10**, 068 (2021). arXiv:2107.10268 [hep-ph]
48. T. Li, J.A. Maxin, D.V. Nanopoulos. arXiv:2107.12843 [hep-ph]
49. S. Li, Y. Xiao, J.M. Yang, Nucl. Phys. B **974**, 115629 (2022). arXiv:2108.00359 [hep-ph]
50. J.L. Lamborn, T. Li, J.A. Maxin, D.V. Nanopoulos, JHEP **11**, 081 (2021). arXiv:2108.08084 [hep-ph]

51. O. Fischer, B. Mellado, S. Antusch, E. Bagnaschi, S. Banerjee, G. Beck, B. Belfatto, M. Bellis, Z. Berezhiani, M. Blanke et al. arXiv:2109.06065 [hep-ph]
52. A.K. Forster, S.F. King. arXiv:2109.10802 [hep-ph]
53. W. Ke, P. Slavich. arXiv:2109.15277 [hep-ph]
54. J. Ellis, J.L. Evans, N. Nagata, D.V. Nanopoulos, K.A. Olive. arXiv:2110.06833 [hep-ph]
55. P. Athron, C. Balázs, D. Jacob, W. Kotlarski, D. Stöckinger, H. Stöckinger-Kim. arXiv:2110.07156 [hep-ph]
56. M. Chakraborti, S. Heinemeyer, I. Saha. arXiv:2111.00322 [hep-ph]
57. S. Chapman. arXiv:2112.04469 [hep-ph]
58. A. Aboubrahim, M. Klasen, P. Nath, R.M. Syed. arXiv:2112.04986 [hep-ph]
59. I. Antoniadis, F. Rondeau. arXiv:2112.07587 [hep-th]
60. J.T. Acuña, P. Stengel, P. Ullio. arXiv:2112.08992 [hep-ph]
61. M.I. Ali, M. Chakraborti, U. Chattopadhyay, S. Mukherjee. arXiv:2112.09867 [hep-ph]
62. A. Djouadi, J.C. Criado, N. Koivunen, K. Müürsepp, M. Raidal, H. Veermäe. arXiv:2112.12502 [hep-ph]
63. K. Wang, J. Zhu. arXiv:2112.14576 [hep-ph]
64. F. Wang, W. Wang, J.M. Yang, Y. Zhang, B. Zhu. arXiv:2201.00156 [hep-ph]
65. M. Chakraborti, S. Heinemeyer, I. Saha. arXiv:2201.03390 [hep-ph]
66. M.A. Boussejra, F. Mahmoudi, G. Uhlrich. arXiv:2201.04659 [hep-ph]
67. R. Dermisek. arXiv:2201.06179 [hep-ph]
68. J. Cao, J. Lian, Y. Pan, Y. Yue, D. Zhang. arXiv:2201114f90 [hep-ph]
69. M.E. Gomez, Q. Shafi, A. Tiwari, C.S. Un. arXiv:2202.06419 [hep-ph]
70. W. Ahmed, I. Khan, T. Li, S. Raza, W. Zhang. arXiv:2202.11011 [hep-ph]
71. A. Chatterjee, A. Datta, S. Roy. arXiv:2202.12476 [hep-ph]
72. M. Chakraborti, S. Iwamoto, J.S. Kim, R. Masełek, K. Sakurai. arXiv:2202.12928 [hep-ph]
73. K. Agashe, M. Ekhterachian, Z. Liu, R. Sundrum. arXiv:2203.01796 [hep-ph]
74. P. Athron, C. Balazs, A. Fowlie, H. Lv, W. Su, L. Wu, J.M. Yang, Y. Zhang. arXiv:2203.04828 [hep-ph]
75. M. Endo, K. Hamaguchi, S. Iwamoto, S.I. Kawada, T. Kitahara, T. Moroi, T. Suehara. arXiv:2203.07056 [hep-ph]
76. S. Chigusa, T. Moroi, Y. Shoji. arXiv:2203.08062 [hep-ph]
77. L. Shang, X. Zhang, Z. Heng. arXiv:2204.00182 [hep-ph]
78. K. Hamaguchi, N. Nagata, M.E. Ramirez-Quezada, JHEP **10**, 088 (2022). arXiv:2204.02413 [hep-ph]
79. X.K. Du, Z. Li, F. Wang, Y.K. Zhang. arXiv:2204.04286 [hep-ph]
80. T.P. Tang, M. Abdughani, L. Feng, Y.L.S. Tsai, Y.Z. Fan. arXiv:2204.04356 [hep-ph]
81. J.M. Yang, Y. Zhang. arXiv:2204.04202 [hep-ph]
82. J. Cao, F. Li, J. Lian, Y. Pan, D. Zhang. arXiv:2204.04710 [hep-ph]
83. P. Athron, M. Bach, D.H.J. Jacob, W. Kotlarski, D. Stöckinger, A. Voigt. arXiv:2204.05285 [hep-ph]
84. R. Masełek. arXiv:2205.04378 [hep-ph]
85. S. Li, Z. Li, F. Wang, J.M. Yang. arXiv:2205.15153 [hep-ph]
86. J. Dickinson, S. Bein, S. Heinemeyer, J. Hiltbrand, J. Hirschauer, W. Hopkins, E. Lipeles, M. Mrowietz, N. Strobbe. arXiv:2207.05103 [hep-ph]
87. M.D. Zheng, F.Z. Chen, H.H. Zhang, Eur. Phys. J. C **82**(10), 895 (2022). arXiv:2207.07636 [hep-ph]
88. T.N. Dao, D.N. Le, M. Mühlleitner, Eur. Phys. J. C **82**(10), 954 (2022). arXiv:2207.12618 [hep-ph]
89. S. Heinemeyer. arXiv:2207.14809 [hep-ph]
90. F. Domingo, U. Ellwanger, C. Hugonie, Eur. Phys. J. C **82**(11), 1074 (2022). arXiv:2209.03863 [hep-ph]
91. J. Cao, X. Jia, L. Meng, Y. Yue, D. Zhang, JHEP **03**, 198 (2023). arXiv:2210.08769 [hep-ph]
92. A. Datta, M. Guchait, A. Roy, S. Roy. arXiv:2211.05905 [hep-ph]
93. J.M. Yang, P. Zhu, R. Zhu, PoS **LHCP2022**, 069 (2022). arXiv:2211.06686 [hep-ph]
94. X. Wang, S.M. Zhao, X.X. Long, Y.T. Wang, T.T. Wang, H.B. Zhang, T.F. Feng, R.X. Zhang. arXiv:2211.10848 [hep-ph]
95. J. Zhao, J. Zhu, P. Zhu, R. Zhu, Phys. Rev. D **107**(5), 055030 (2023). arXiv:2211.14587 [hep-ph]
96. M. Chakraborti, S. Heinemeyer, I. Saha, Int. J. Mod. Phys. A **37**(30), 2246010 (2022)
97. P. Borah, P. Ghosh, S. Roy, A.K. Saha. arXiv:2301.05061 [hep-ph]
98. M.A. Ajaib, F. Nasir. arXiv:2302.02047 [hep-ph]
99. S. Baum, M. Carena, T. Ou, D. Rocha, N.R. Shah, C.E.M. Wagner. arXiv:2303.01523 [hep-ph]
100. C. Salih Un, M.E. Gomez, Q. Shafi, A. Tiwari, LHEP **2023**, 360 (2023)
101. Y. He, X. Jia, L. Meng, Y. Yue, D. Zhang. arXiv:2303.02360 [hep-ph]
102. A. Mukherjee, S. Niyogi, S. Poddar, J.P. Saha. arXiv:2303.05144 [hep-ph]
103. H. Kulkarni, S. Raby, JHEP **05**, 152 (2023). arXiv:2303.07209 [hep-ph]
104. Z.J. Yang, T.F. Feng, X.G. Wu. arXiv:2303.11645 [hep-ph]
105. W. Zhang, W. Ahmed, I. Khan, T. Li, S. Raza. arXiv:2304.01082 [hep-ph]
106. M.E. Gomez, S. Lola, Q. Shafi, A. Tiwari, C. Salih Un, LHEP **2023**, 381 (2023)
107. L.J. Jia, Z. Li, F. Wang, Universe **9**(5), 214 (2023). arXiv:2305.04623 [hep-ph]
108. A. Choudhury, S. Mitra, A. Mondal, S. Mondal. arXiv:2305.15211 [hep-ph]
109. J. Cao, L. Meng, Y. Yue. arXiv:2306.06854 [hep-ph]
110. N. Aghanim et al. [Planck Collaboration], Astron. Astrophys. **641**, A6 (2020). arXiv:1807.06209 [astro-ph.CO]. [erratum: Astron. Astrophys. 652 (2021), C4]
111. E. Aprile et al. [XENON Collaboration], Phys. Rev. Lett. **121**(11), 111302 (2018). arXiv:1805.12562 [astro-ph.CO]
112. D.S. Akerib et al. [LUX Collaboration], Phys. Rev. Lett. **118**(2), 021303 (2017). arXiv:1608.07648 [astro-ph.CO]
113. X. Cui et al. [PandaX-II Collaboration], Phys. Rev. Lett. **119**(18), 181302 (2017). arXiv:1708.06917 [astro-ph.CO]
114. See: https://twiki.cern.ch/twiki/bin/view/AtlasPublic/SupersymmetryPublicResults
115. See: https://twiki.cern.ch/twiki/bin/view/CMSPublic/PhysicsResultsSUS
116. S. Heinemeyer, W. Hollik, D. Stöckinger, A.M. Weber, G. Weiglein, JHEP **08**, 052 (2006). arXiv:hep-ph/0604147
117. S. Heinemeyer, W. Hollik, A.M. Weber, G. Weiglein, JHEP **04**, 039 (2008). arXiv:0710.2972 [hep-ph]
118. S. Heinemeyer, W. Hollik, G. Weiglein, L. Zeune, JHEP **12**, 084 (2013). arXiv:1311.1663 [hep-ph]
119. S. Heinemeyer, F. von der Pahlen. arXiv:2302.12187 [hep-ph]
120. S. Heinemeyer, F. von der Pahlen, PoS **LL2022**, 077 (2022). arXiv:2304.12892 [hep-ph]
121. J.R. Ellis, D.V. Nanopoulos, Phys. Lett. B **110**, 44–48 (1982)
122. R. Barbieri, R. Gatto, Phys. Lett. B **110**, 211 (1982)
123. A.H. Chamseddine, R.L. Arnowitt, P. Nath, Phys. Rev. Lett. **49**, 970 (1982)
124. J.R. Ellis, K.A. Olive, Y. Santoso, V.C. Spanos, Phys. Lett. B **565**, 176–182 (2003). arXiv:hep-ph/0303043
125. H. Baer, C. Balazs, A. Belyaev, T. Krupovnickas, X. Tata, JHEP **06**, 054 (2003). arXiv:hep-ph/0304303
126. A.B. Lahanas, D.V. Nanopoulos, Phys. Lett. B **568**, 55–62 (2003). arXiv:hep-ph/0303130

127. U. Chattopadhyay, A. Corsetti, P. Nath, Phys. Rev. D **68**, 035005 (2003). arXiv:hep-ph/0303201
128. J.R. Ellis, K.A. Olive, Y. Santoso, Phys. Lett. B **539**, 107–118 (2002). arXiv:hep-ph/0204192
129. E. Bagnaschi et al., Eur. Phys. J. C **78**(3), 256 (2018). arXiv:1710.11091 [hep-ph]
130. K.J. de Vries, E.A. Bagnaschi et al., Eur. Phys. J. C **75**(9), 422 (2015). arXiv:1504.03260 [hep-ph]
131. J.F. Gunion, H.E. Haber, M. Sher, Nucl. Phys. B **306**, 1–13 (1988)
132. J.A. Casas, A. Lleyda, C. Munoz, Nucl. Phys. B **471**, 3–58 (1996). arXiv:hep-ph/9507294
133. U. Chattopadhyay, A. Dey, JHEP **11**, 161 (2014). https://doi.org/10.1007/JHEP11(2014)161. arXiv:1409.0611 [hep-ph]
134. W.G. Hollik, G. Weiglein, J. Wittbrodt, JHEP **03**, 109 (2019). https://doi.org/10.1007/JHEP03(2019)109. arXiv:1812.04644 [hep-ph]
135. P. Slavich, S. Heinemeyer (eds.), E. Bagnaschi et al., Eur. Phys. J. C **81**(5), 450 (2021). arXiv:2012.15629 [hep-ph]
136. T. Aoyama et al., Phys. Rep. **887**, 1–166 (2020). arXiv:2006.04822 [hep-ph]
137. T. Aoyama, M. Hayakawa, T. Kinoshita, M. Nio, Phys. Rev. Lett. **109**, 111808 (2012). arXiv:1205.5370 [hep-ph]
138. T. Aoyama, T. Kinoshita, M. Nio, Atoms **7**(1), 28 (2019)
139. A. Czarnecki, W.J. Marciano, A. Vainshtein, Phys. Rev. D **67**, 073006 (2003). arXiv:hep-ph/0212229
140. C. Gnendiger, D. Stöckinger, H. Stöckinger-Kim, Phys. Rev. D **88**, 053005 (2013). arXiv:1306.5546 [hep-ph]
141. M. Davier, A. Hoecker, B. Malaescu, Z. Zhang, Eur. Phys. J. C **77**(12), 827 (2017). arXiv:1706.09436 [hep-ph]
142. A. Keshavarzi, D. Nomura, T. Teubner, Phys. Rev. D **97**(11), 114025 (2018). arXiv:1802.02995 [hep-ph]
143. G. Colangelo, M. Hoferichter, P. Stoffer, JHEP **02**, 006 (2019). arXiv:1810.00007 [hep-ph]
144. M. Hoferichter, B.L. Hoid, B. Kubis, JHEP **08**, 137 (2019). arXiv:1907.01556 [hep-ph]
145. M. Davier, A. Hoecker, B. Malaescu, Z. Zhang, Eur. Phys. J. C **80**(3), 241 (2020). arXiv:1908.00921 [hep-ph]. [erratum: Eur. Phys. J. C 80 (2020) no. 5, 410]
146. A. Keshavarzi, D. Nomura, T. Teubner, Phys. Rev. D **101**(1), 014029 (2020). arXiv:1911.00367 [hep-ph]
147. A. Kurz, T. Liu, P. Marquard, M. Steinhauser, Phys. Lett. B **734**, 144–147 (2014). arXiv:1403.6400 [hep-ph]
148. K. Melnikov, A. Vainshtein, Phys. Rev. D **70**, 113006 (2004). arXiv:hep-ph/0312226
149. P. Masjuan, P. Sanchez-Puertas, Phys. Rev. D **95**(5), 054026 (2017). arXiv:1701.05829 [hep-ph]
150. G. Colangelo, M. Hoferichter, M. Procura, P. Stoffer, JHEP **04**, 161 (2017). arXiv:1702.07347 [hep-ph]
151. M. Hoferichter, B.L. Hoid, B. Kubis, S. Leupold, S.P. Schneider, JHEP **10**, 141 (2018). arXiv:1808.04823 [hep-ph]
152. A. Gérardin, H.B. Meyer, A. Nyffeler, Phys. Rev. D **100**(3), 034520 (2019). arXiv:1903.09471 [hep-lat]
153. J. Bijnens, N. Hermansson-Truedsson, A. Rodríguez-Sánchez, Phys. Lett. B **798**, 134994 (2019). arXiv:1908.03331 [hep-ph]
154. G. Colangelo, F. Hagelstein, M. Hoferichter, L. Laub, P. Stoffer, JHEP **03**, 101 (2020). arXiv:1910.13432 [hep-ph]
155. T. Blum, N. Christ, M. Hayakawa, T. Izubuchi, L. Jin, C. Jung, C. Lehner, Phys. Rev. Lett. **124**(13), 132002 (2020). arXiv:1911.08123 [hep-lat]
156. G. Colangelo, M. Hoferichter, A. Nyffeler, M. Passera, P. Stoffer, Phys. Lett. B **735**, 90–91 (2014). arXiv:1403.7512 [hep-ph]
157. S. Borsanyi et al., Nature **593**(7857), 51–55 (2021). arXiv:2002.12347 [hep-lat]
158. M. Cè et al., Phys. Rev. D **106**(11), 114502 (2022). arXiv:2206.06582 [hep-lat]
159. C. Alexandrou et al. [Extended Twisted Mass], Phys. Rev. D **107**(7), 074506 (2023). arXiv:2206.15084 [hep-lat]
160. C. Lehner, A.S. Meyer, Phys. Rev. D **101**, 074515 (2020). arXiv:2003.04177 [hep-lat]
161. A. Crivellin, M. Hoferichter, C.A. Manzari, M. Montull, Phys. Rev. Lett. **125**(9), 091801 (2020). arXiv:2003.04886 [hep-ph]
162. A. Keshavarzi, W.J. Marciano, M. Passera, A. Sirlin, Phys. Rev. D **102**(3), 033002 (2020). arXiv:2006.12666 [hep-ph]
163. E. de Rafael, Phys. Rev. D **102**(5), 056025 (2020). arXiv:2006.13880 [hep-ph]
164. B. Abi et al. [Muon g-2], Phys. Rev. Lett. **126**(14), 141801 (2021). arXiv:2104.03281 [hep-ex]
165. G.W. Bennett et al. [Muon g-2 Collaboration], Phys. Rev. D **73**, 072003 (2006). arXiv:hep-ex/0602035
166. J.L. Lopez, D.V. Nanopoulos, X. Wang, Phys. Rev. D **49**, 366–372 (1994). arXiv:hep-ph/9308336
167. U. Chattopadhyay, P. Nath, Phys. Rev. D **53**, 1648–1657 (1996). arXiv:hep-ph/9507386
168. U. Chattopadhyay, D.K. Ghosh, S. Roy, Phys. Rev. D **62**, 115001 (2000). arXiv:hep-ph/0006049
169. K. Kowalska, L. Roszkowski, E.M. Sessolo, A.J. Williams, JHEP **06**, 020 (2015). arXiv:1503.08219 [hep-ph]
170. P. von Weitershausen, M. Schafer, H. Stöckinger-Kim, D. Stöckinger, Phys. Rev. D **81**, 093004 (2010). arXiv:1003.5820 [hep-ph]
171. H. Fargnoli, C. Gnendiger, S. Paßehr, D. Stöckinger, H. Stöckinger-Kim, JHEP **1402**, 070 (2014). arXiv:1311.1775 [hep-ph]
172. M. Bach, Jh. Park, D. Stöckinger, H. Stöckinger-Kim, JHEP **1510**, 026 (2015). arXiv:1504.05500 [hep-ph]
173. S. Heinemeyer, D. Stöckinger, G. Weiglein, Nucl. Phys. B **690**, 62–80 (2004). arXiv:hep-ph/0312264
174. S. Heinemeyer, D. Stöckinger, G. Weiglein, Nucl. Phys. B **699**, 103–123 (2004). arXiv:hep-ph/0405255
175. P. Athron et al., Eur. Phys. J. C **76**(2), 62 (2016). arXiv:1510.08071 [hep-ph]
176. P.M. Ferreira, M. Mühlleitner, R. Santos, G. Weiglein, J. Wittbrodt, JHEP **09**, 006 (2019). arXiv:1905.10234 [hep-ph]
177. M. Drees, H. Dreiner, D. Schmeier, J. Tattersall, J.S. Kim, Comput. Phys. Commun. **187**, 227–265 (2015). arXiv:1312.2591 [hep-ph]
178. J.S. Kim, D. Schmeier, J. Tattersall, K. Rolbiecki, Comput. Phys. Commun. **196**, 535–562 (2015). arXiv:1503.01123 [hep-ph]
179. D. Dercks, N. Desai, J.S. Kim, K. Rolbiecki, J. Tattersall, T. Weber, Comput. Phys. Commun. **221**, 383–418 (2017). arXiv:1611.09856 [hep-ph]
180. G. Aad et al. [ATLAS], Phys. Rev. D **101**(7), 072001 (2020). arXiv:1912.08479 [hep-ex]
181. G. Aad et al. [ATLAS], Eur. Phys. J. C **81**(12), 1118 (2021). arXiv:2106.01676 [hep-ex]
182. G. Aad et al. [ATLAS Collaboration], Eur. Phys. J. C **80**(2), 123 (2020). arXiv:1908.08215 [hep-ex]
183. G. Aad et al. [ATLAS], Phys. Rev. D **101**(3), 032009 (2020). arXiv:1911.06660 [hep-ex]
184. CMS. arXiv:2207.02254 [hep-ex]
185. [ATLAS], ATLAS-CONF-2023-029
186. A.M. Sirunyan et al. [CMS], Phys. Rev. Lett. **124**(4), 041803 (2020). arXiv:1910.01185 [hep-ex]
187. J.J. Heinrich [ATLAS], PhD thesis: "Search for charged stable massive particles with the ATLAS detector. https://doi.org/10.5282/edoc.22183.
188. M. Aaboud et al. [ATLAS], Phys. Rev. D **99**(9), 092007 (2019). arXiv:1902.01636 [hep-ex]
189. G. Aad et al. [ATLAS], Eur. Phys. J. C **82**(7), 606 (2022). arXiv:2201.02472 [hep-ex]

190. CMS, Proton–proton collisions at 13 TeV, CMS-PAS-SUS-21-006
191. G. Aad et al. [ATLAS], Phys. Rev. Lett. **127**(5), 051802 (2021). arXiv:2011.07812 [hep-ex]
192. G. Belanger, F. Boudjema, A. Pukhov, A. Semenov, Comput. Phys. Commun. **149**, 103–120 (2002). arXiv:hep-ph/0112278
193. G. Belanger, F. Boudjema, A. Pukhov, A. Semenov, Comput. Phys. Commun. **176**, 367–382 (2007). arXiv:hep-ph/0607059
194. G. Belanger, F. Boudjema, A. Pukhov, A. Semenov, Comput. Phys. Commun. **177**, 894–895 (2007)
195. G. Belanger, F. Boudjema, A. Pukhov, A. Semenov. arXiv:1305.0237 [hep-ph]
196. J. Aalbers et al. [LZ]. arXiv:2207.03764 [hep-ex]
197. T.R. Slatyer. arXiv:1710.05137 [hep-ph]
198. A. Hryczuk, K. Jodlowski, E. Moulin, L. Rinchiuso, L. Roszkowski, E.M. Sessolo, S. Trojanowski, JHEP **10**, 043 (2019). arXiv:1905.00315 [hep-ph]
199. L. Rinchiuso, O. Macias, E. Moulin, N.L. Rodd, T.R. Slatyer, Phys. Rev. D **103**(2), 023011 (2021). arXiv:2008.00692 [astro-ph.HE]
200. R.T. Co, B. Sheff, J.D. Wells. arXiv:2105.12142 [hep-ph]
201. A. McDaniel, M. Ajello, C.M. Karwin, M. Di Mauro, A. Drlica-Wagner, M. Sànchez-Conde. arXiv:2311.04982 [astro-ph.HE]
202. M. Ackermann et al. [Fermi-LAT], Phys. Rev. Lett. **115**(23), 231301 (2015). arXiv:1503.02641 [astro-ph.HE]
203. M. Chakraborti, U. Chattopadhyay, A. Choudhury, A. Datta, S. Poddar, JHEP **07**, 019 (2014). arXiv:1404.4841 [hep-ph]
204. H. Baer, V. Barger, H. Serce, Phys. Rev. D **94**(11), 115019 (2016). arXiv:1609.06735 [hep-ph]
205. A. Djouadi, J.L. Kneur, G. Moultaka, Comput. Phys. Commun. **176**, 426 (2007). arXiv:hep-ph/0211331
206. J.L. Kneur, G. Moultaka, M. Ughetto, D. Zerwas, A. Djouadi, Comput. Phys. Commun. **291**, 108805 (2023). arXiv:2211.16956 [hep-ph]
207. Joint LEP2 SUSY Working Group, the ALEPH, DELPHI, L3 and OPAL Collaborations. See: http://lepsusy.web.cern.ch/lepsusy/
208. M. Mühlleitner, A. Djouadi, Y. Mambrini, Comput. Phys. Commun. **168**, 46 (2005). arXiv:hep-ph/0311167
209. J.R. Ellis, T. Falk, G. Ganis, K.A. Olive, M. Srednicki, Phys. Lett. B **510**, 236–246 (2001). arXiv:hep-ph/0102098
210. J. Hisano, S. Matsumoto, M.M. Nojiri, O. Saito, Phys. Rev. D **71**, 015007 (2005). arXiv:hep-ph/0407168
211. G. Aad et al. [ATLAS], Phys. Rev. Lett. **125**(5), 051801 (2020). arXiv:2002.12223 [hep-ex]
212. E. Bagnaschi et al., Eur. Phys. J. C **79**(7), 617 (2019). arXiv:1808.07542 [hep-ph]
213. P. Bechtle, O. Brein, S. Heinemeyer, G. Weiglein, K.E. Williams, Comput. Phys. Commun. **181**, 138–167 (2010). arXiv:0811.4169 [hep-ph]
214. P. Bechtle, O. Brein, S. Heinemeyer, G. Weiglein, K.E. Williams, Comput. Phys. Commun. **182**, 2605–2631 (2011). arXiv:1102.1898 [hep-ph]
215. P. Bechtle, O. Brein, S. Heinemeyer, O. Stål, T. Stefaniak, G. Weiglein, K.E. Williams, Eur. Phys. J. C **74**(3), 2693 (2014). arXiv:1311.0055 [hep-ph]
216. P. Bechtle, S. Heinemeyer, O. Stål, T. Stefaniak, G. Weiglein, Eur. Phys. J. C **75**(9), 421 (2015). arXiv:1507.06706 [hep-ph]
217. P. Bechtle, D. Dercks, S. Heinemeyer, T. Klingl, T. Stefaniak, G. Weiglein, J. Wittbrodt, Eur. Phys. J. C **80**(12), 1211 (2020). arXiv:2006.06007 [hep-ph]
218. H. Bahl, T. Biekötter, S. Heinemeyer, C. Li, S. Paasch, G. Weiglein, J. Wittbrodt, Comput. Phys. Commun. **291**, 108803 (2023). arXiv:2210.09332 [hep-ph]
219. [CMS]. arXiv:2208.02717 [hep-ex]
220. T. Jittoh, J. Sato, T. Shimomura, M. Yamanaka, Phys. Rev. D **73**, 055009 (2006). arXiv:hep-ph/0512197 [hep-ph]. [erratum: Phys. Rev. D 87 (2013) no. 1, 019901]
221. M. Citron, J. Ellis, F. Luo, J. Marrouche, K.A. Olive, K.J. de Vries, Phys. Rev. D **87**(3), 036012 (2013). arXiv:1212.2886 [hep-ph]
222. M. Kawasaki, K. Kohri, T. Moroi, Phys. Rev. D **71**, 083502 (2005). arXiv:astro-ph/0408426
223. [CMS], CMS-PAS-EXO-16-036
224. D.S. Akerib et al. [LUX-ZEPLIN], Phys. Rev. D **101**(5), 052002 (2020). arXiv:1802.06039 [astro-ph.IM]
225. E. Aprile et al. [XENON], JCAP **11**, 031 (2020). arXiv:2007.08796 [physics.ins-det]
226. C.E. Aalseth [DarkSide-20k], Eur. Phys. J. Plus **133**, 131 (2018). arXiv:1707.08145 [physics.ins-det]
227. J. Billard et al. arXiv:2104.07634 [hep-ex]
228. F. Ruppin, J. Billard, E. Figueroa-Feliciano, L. Strigari, Phys. Rev. D **90**(8), 083510 (2014). arXiv:1408.3581 [hep-ph]
229. X. Cid Vidal et al. [CERN Yellow Rep], Monogr **7**, 585–865 (2019). arXiv:1812.07831 [hep-ph]
230. H. Baer et al., The International Linear Collider Technical Design Report—Volume 2: Physics. arXiv:1306.6352 [hep-ph]
231. G. Moortgat-Pick et al., Eur. Phys. J. C **75**(8), 371 (2015). arXiv:1504.01726 [hep-ph]
232. L. Linssen, A. Miyamoto, M. Stanitzki, H. Weerts. arXiv:1202.5940 [physics.ins-det]
233. H. Abramowicz et al. [CLIC Detector and Physics Study Collaboration]. arXiv:1307.5288 [hep-ex]
234. P. Burrows et al. [CLICdp and CLIC Collaborations], CERN Yellow Rep. Monogr. **1802**, 1 (2018). arXiv:1812.06018 [physics.acc-ph]
235. B. Fuks, M. Klasen, D.R. Lamprea, M. Rothering, Eur. Phys. J. C **73**, 2480 (2013). arXiv:1304.0790 [hep-ph]
236. G. Bozzi, B. Fuks, M. Klasen, Phys. Rev. D **74**, 015001 (2006). arXiv:hep-ph/0603074
237. G. Bozzi, B. Fuks, M. Klasen, Nucl. Phys. B **777**, 157–181 (2007). arXiv:hep-ph/0701202
238. J. Debove, B. Fuks, M. Klasen, Phys. Lett. B **688**, 208–211 (2010). arXiv:0907.1105 [hep-ph]
239. J. Debove, B. Fuks, M. Klasen, Nucl. Phys. B **842**, 51–85 (2011). arXiv:1005.2909 [hep-ph]
240. T. Barklow, J. Brau, K. Fujii, J. Gao, J. List, N. Walker, K. Yokoya. arXiv:1506.07830 [hep-ex]
241. K. Fujii et al. arXiv:1710.07621 [hep-ex]
242. S. Heinemeyer, C. Schappacher, Eur. Phys. J. C **77**(9), 649 (2017). arXiv:1704.07627 [hep-ph]
243. S. Heinemeyer, C. Schappacher, Eur. Phys. J. C **78**(7), 536 (2018). arXiv:1803.10645 [hep-ph]
244. T. Fritzsche, T. Hahn, S. Heinemeyer, F. von der Pahlen, H. Rzehak, C. Schappacher, Comput. Phys. Commun. **185**, 1529–1545 (2014). arXiv:1309.1692 [hep-ph]
245. M. Berggren. arXiv:1308.1461 [hep-ph]
246. M.T.N. Pardo de Vera, M. Berggren, J. List. arXiv:2002.01239 [hep-ph]
247. M. Berggren. arXiv:2003.12391 [hep-ph]
248. D.P. Aguillard et al. [Muon g-2]. arXiv:2308.06230 [hep-ex]